The Role of Environmental Shear and Thermodynamic Conditions in Determining the Structure and Evolution of Mesoscale Convective Systems during TOGA COARE

MARGARET A. LEMONE

National Center for Atmospheric Research, Boulder, Colorado*

EDWARD J. ZIPSER

Department of Meteorology, Texas A&M University, College Station, Texas

STANLEY B. TRIER

National Center for Atmospheric Research, Boulder, Colorado

(Manuscript received 26 March 1997, in final form 10 March 1998)

ABSTRACT

A collection of case studies is used to elucidate the influence of environmental soundings on the structure and evolution of the convection in the mesoscale convective systems sampled by the turboprop aircraft in the Tropical Ocean Global Atmosphere (TOGA) Coupled Ocean–Atmosphere Response Experiment (COARE). The soundings were constructed primarily from aircraft data below 5–6 km and primarily from radiosonde data at higher altitudes.

The well-documented role of the vertical shear of the horizontal wind in determining the mesoscale structure of tropical convection is confirmed and extended. As noted by earlier investigators, nearly all convective bands occurring in environments with appreciable shear below a low-level wind maximum are oriented nearly normal to the shear beneath the wind maximum and propagate in the direction of the low-level shear at a speed close to the wind maximum; when there is appreciable shear at middle levels (800–400 mb), convective bands form parallel to the shear. With appreciable shear at both levels, the lower-level shear determines the orientation of the primary convective bands. If the midlevel shear is opposite the low-level shear, secondary bands parallel to the midlevel shear will extend rearward from the primary band in later stages of its evolution; if the midlevel shear is 90 degrees to the low-level shear, the primary band will retain its two-dimensional mesoscale structure. Convection has no obvious mesoscale organization on days with little shear or days with widespread convection.

Environmental temperatures and humidities have no obvious effect on the mesoscale convective pattern, but they affect COARE convection in other ways. The high tops of COARE convection are related to high parcel equilibrium levels, which approach 100 mb in some cases. Convective available potential energies are larger than those in the GARP (Global Atmospheric Research Program) Atlantic Tropical Experiment (GATE) mainly because of the higher equilibrium levels. The buoyancy integrated over the lowest 500 mb is similar for the two experiments. Convective inihibitions are small, enabling convection to propagate with only weak forcing. Comparison of slow-moving shear-parallel bands in COARE and GATE suggests that lower relative humidities between the top of the mixed layer and 500 mb can shorten their lifetimes significantly.

COARE mesoscale organization and evolution differs from what was observed in GATE. Less-organized convection is more common in COARE. Of the convective bands observed, a greater fraction in COARE are faster-moving, shear-perpendicular squall lines. GATE slow-moving lines tend to be longer lived than those for COARE. The differences are probably traceable to differences in environmental shear and relative humidity, respectively.

1. Introduction

Two of the four major objectives of the Tropical Ocean Global Atmosphere (TOGA) Coupled Atmosphere–Ocean Response Experiment (COARE) dealt with the mechanisms organizing deep, precipitating convection and its effects on the surrounding atmosphere and the ocean beneath (Webster and Lukas 1992). We focus on the influence of environmental conditions, as defined by vertical soundings, on the structure and evolution of convection on the mesoscale. More precisely, if a mesoscale convective system (MCS) is considered as a 100+ km scale entity consisting of convective cloud and stratiform cloud mainly produced by the convection, we focus on the structure and evolution of the convection. For more information on the stratiform portions of COARE MCSs, the reader is referred to Rickenbach and Rutledge (1998) and Kingsmill and Houze (1998a,b).

* The National Center for Atmospheric Research is sponsored by the National Science Foundation.

Corresponding author address: Dr. Margaret A. LeMone, NCAR, P.O. Box 3000, Boulder, CO 80307.
E-mail: lemone@ucar.edu

Mesoscale organization of convection impacts the kinematic structure and longevity of MCSs, and by implication the associated momentum transports, surface thermodynamic fluxes and stress, and radiative fluxes at the top of the system. The observational studies of LeMone (1983) and LeMone et al. (1984b), and theoretical studies of Moncrieff (1978, 1981), demonstrate that the degree of linear convective organization determines the nature of the momentum transport. Although random convection will mix momentum vertically through its depth, convection organized into bands will often *increase* the magnitude of the vertical shear of the horizontal wind normal to the band axis. The nature of this momentum transport is related to first order to the familiar front-to-rear updraft and rear-to-front downdraft associated with squall lines at least since Newton's (1950) seminal work. In contrast, the component of horizontal momentum parallel to the convective-band axis seems to be transported as a passive scalar, which usually results in a decrease in the vertical shear of that component (LeMone et al. 1984b; LeMone and Moncrieff 1994). LeMone and Moncrieff also note the role of band structure in the rate of anvil and subcloud cold-pool growth. In addition, MCS momentum transport, thermodynamic transport, and rainfall affect the strength of the surface fluxes. Thus MCS structure and evolution affects vertical transports, the radiation budget, and sea–air transfer. MCS longevity determines the duration and aerial extent of their impact.

Historically, linear organization of convection was associated with strong larger-scale structures, such as fronts and developing cyclones, a view that is clearly valid, as illustrated by the extension of the classic diagrams of clouds and precipitation associated with fronts and developing cyclones to include MCS structure and evolution (e.g., Newton 1963; Carbone 1982; Hobbs and Persson 1982; Koch 1984). The strong forcing associated with these larger-scale systems has to be considered along with their characteristic vertical profiles of horizontal wind to explain the observed geographically systematic orientations of Oklahoma squall lines noted by Bluestein and Jain (1985), Bluestein et al. (1987), and Houze et al. (1990).

However, over the last 25 years, there has been an increased realization that convection can be organized on the mesoscale without preexisting mesoscale forcing structures such as fronts. That is, structure and evolution can be determined by environmental wind, temperature, and humidity profiles whose horizontal variation is on a large enough scale that they could be considered horizontally uniform. We call this *self-organization*. For example, Moncrieff and collaborators (Moncrieff and Green 1972, Moncrieff and Miller 1976; Moncrieff 1978) combined vertical shear with the convective available potential energy (CAPE) into a Richardson number to distinguish types of convection (most significantly, linear vs cellular). Support for self-organization quickly came from numerical models initialized by single soundings. For example, Weisman and Klemp (1982, 1984, 1986) associated the formation of squall-line convection with stronger shears through the lowest 2–3 km. They also found that shear through a deeper layer favors strong, persistent cells called supercells for a certain range of their Richardson number.

In parallel, several observational studies based on tropical field programs have indicated a strong association between environmental wind profiles and the orientation of convective bands. Barnes and Sieckman (1984) described two classes of convective systems over the tropical Atlantic in the GATE[1], so-called fast- and slow-movers. Fast-movers occurred for wind profiles with strong low-level shear and a low-level jet and tended to be nearly normal to the low-level shear at speeds $c \geq 7$ m s^{-1}, while slow-movers ($c \leq 3$ m s^{-1}) occurred with weak low-level shear and were parallel to the shear from ~1 to 6 km (~900 to 500 mb). Similar behavior was noted in EMEX[2] by Alexander and Young (1992), but with slow-movers parallel to the shear between 800 and 400 mb. Fast-movers (herein also called squall lines) have been studied far more than slow-movers, with similar results to the cited works: an environmental low-level jet with strong shear beneath, line orientation perpendicular to the low-level shear, and a leading-edge speed corresponding to the maximum earth-relative line-normal wind. Significantly, other observational studies showing this relationship are also from the Tropics: in Venezuela (Betts et al. 1976) and along the northern border of Australia (Keenan and Carbone 1992).

The studies mentioned in the foregoing suggest that self-organization is an important if not the dominant mechanism organizing convection in the Tropics. However, the number of samples in each study is small; as Alexander and Young (1992) note, the observed range of environmental conditions, particularly thermodynamics, is limited. Furthermore, none of the classification schemes allow for the more complex, yet still ordered, structure observed for the COARE systems. Finally, differences in the evolution of ''shear-parallel lines'' in GATE and COARE are not accounted for in the classification schemes of Barnes and Sieckman (1984) and Alexander and Young (1992).

This work is thus an extension of previous studies of the relationship of environmental soundings to the structure and evolution of mesoscale convection in the Tropics. In particular we will (i) define environmental conditions conducive to persistent linear convection and (ii) determine how this convection aligns relative to the environmental wind. We focus on MCS convection sampled by the turboprop aircraft (the two NOAA P3s and the NCAR Electra) in TOGA COARE. These MCSs

[1] GATE: (Global Atmospheric Research Program) Atlantic Tropical Experiment, conducted in the tropical Atlantic in 1974.

[2] EMEX: Equatorial Mesoscale EXperiment, conducted north of Australia in 1987.

have reflectivity patterns of the order of 100–300 km in the largest horizontal dimension. The MCSs fit in the categories class I and greater in the Mapes and Houze (1993) classification, implying satellite cold (<208 K) cloud areas of at least 6000 km^2 (Webster and Lukas 1992). Typically, we observe these systems in their mature to decaying phases. We do not address the conditions leading to the convective system(s) producing the much larger cloud shields identified as ''superclusters'' by Nakazawa (1988), Lau et al. (1989), and others. Indeed, we have found single soundings not to be very illuminating in this context.

Data analysis procedures are summarized in section 2. We relate the observed convection to environmental winds and thermodynamics in section 3. We compare COARE MCS convection to GATE MCS convection and offer some explanations for the differences in section 4, and we summarize our conclusions in section 5.

2. Data analysis

a. Definition of ''inflow environment''

We consider a sounding ''inflow environment'' for an MCS if the air at the lowest levels has a relative flow component toward the convection and if this low-level air has the characteristics of a fair-weather boundary layer. That is, (i) the sounding was on the low-level inflow side and less than ~150 km from the convection of interest, (ii) there was no liquid water below 400 m as indicated by in situ measurements or apparent sea surface temperature (which drops when the aircraft is passing through or over cloud or rain), and (iii) there was a well-defined mixed layer (near-uniform potential temperature θ and specific humidity q) more than 300 m deep.

This definition is consistent with a study of convection that is self-organized in response to an environment that can be specified by a single sounding. Thus, for example, on days with widespread convection, we restrict ourselves to the convection on the edge, recognizing that the environment of convection in the interior is too complex. Even in this simpler outer environment, or for isolated MCSs, there can be scattered smaller convective systems or leftover cold pools on the inflow side. Our reasons for not counting these in the environmental soundings are (i) numerical simulations (Trier et al. 1996; Skamarock et al. 1996) of two types of system in COARE suggest that our definition of inflow environment is a useful one for cloud models initiated with a single sounding; (ii) aircraft did not systematically sample the environment, and thus appropriate weighting of the modified air is difficult, particularly for momentum; and (iii) we expect the unmodified air to penetrate the farthest vertically in convection, whereas modified air would contribute more in a negative way (e.g., producing gaps in the convection). However, we recognize that storm dynamics sometimes affect inflow air and will discuss a few examples where the convective band has apparently modified the vertical shear in the nearby boundary layer.

b. Construction of soundings

Environmental soundings are typically based on aircraft measurements between 30 m and 6 km above mean sea level (MSL) (~1005–500 hPa) and radiosonde data from 6 km to 100 mb (~16 km). On rare occasions, surface data and dropsonde data were used. Aircraft provided the best low-level data because they were closer to the system of interest and because radiosondes had significant humidity biases at low levels (Zipser and Johnson 1998). The humidity problem was less significant above 6 km.

1) LOWEST KILOMETER

For the lowest kilometer, the temperature, dewpoint, equivalent potential temperature θ_e, winds, apparent SST, and cloud liquid water were plotted for all aircraft soundings and low-level (below 400 m) legs, and located relative to the convection. Those meeting the criteria for ''environmental'' were selected for the composite. Mixed-layer soundings that were disqualified simply because they did not extend upward to the mixed-layer top were added if they were through a deep enough layer (≥200–300 m) to enable vertical extrapolation. For an individual convective system, the number of environmental aircraft soundings varied from none at all (when entry and exit soundings were in modified air) to over 20. Most of the time, the rejected soundings were those flown in the modified air within or behind the convection of interest, but there were also soundings near the leading edge with modified vertical shear within the lowest few hundred meters (see section 4a), or soundings sufficiently far from the selected target that they were not considered relevant. Aircraft horizontal-leg data and, rarely, surface data were used in the absence of adequate low-level soundings.

All environmental soundings within the mixed layer were used to determine the horizontally averaged mixed-layer properties for each case. The environmental soundings deep enough to include the mixed-layer top were used to determine the average mixed-layer depth. The thermodynamics from these soundings were combined with those of the shallower soundings to form the average. To ensure an equal number of points at each level, the temperatures and dewpoints from the shallower soundings were extrapolated downward to the surface and upward to the average mixed-layer top, assuming an adiabatic lapse rate and a linearly varying dewpoint. Aircraft soundings suggested that downward extrapolation within the mixed layer was valid to ~30 m; the profile formulations of Fairall et al. (1996) can be used to improve estimates below that height.

Boundary layer winds were more problematic. On

TABLE 1. Comparison of aircraft data for selected days with convection (H: *NOAA42*, I: *NOAA43*, E: NCAR Electra). The x's denote a lack of intercomparision data (aircraft not present, or fields too nonuniform).

Date	T (K) (H–I)	Td (K) (H–I)	SST (K) (H–I)	T (K) (E–I)	Td (K) (E–I)	SST (K) (E–I)
19 Nov	0.00	0.50	x	x	x	x
26 Nov	−0.40	0.70	−0.10	x	x	x
14 Dec	x	x	x	0.40	0.50	1.00
9 Jan	−0.30	0.60	0.10	x	x	x
17 Jan	x	0.80	0.10	0.35	0.40	1.20
18 Jan	−0.10	0.75	~0	x	x	x
10 Feb	−0.10	1.35	−0.50	0.60	0.30	0.70
20 Feb	−0.15	0.67	−0.87	x	x	x
22 Feb	−0.10	0.50	−0.90	x	x	x

some days with more complex convection or >150 km boundary layer legs not fixed to one convective system, there was considerable horizontal variation (up to 4 m s^{-1} horizontally) in the unmodified air. In such cases, we focused on the inflow environment of one convective target, and used the boundary layer vertical shear when it was more consistent than the actual wind.

2) BETWEEN 1 AND 5–6 KM

Data from 1 km to 5–6 km MSL were typically from soundings taken by one or more aircraft upon entry or exit from the area. When the deep soundings were both environmental but differed, we used the earlier soundings, and those on the inflow side and closer to the system of interest. If the deep sounding was sufficiently different from the low-level composite, a new composite was constructed giving more weight to the deep sounding. For some days, both aircraft data taken on higher-level legs and dropsonde data were incorporated into these soundings. Dropsondes were crucial when the deep aircraft soundings were taken in modified air.

3) 5–6 KM TO 100 MB (~16 KM)

Data from 5–6 km to 100 mb were obtained from the spatially and temporally closest radiosonde with the temperatures and winds that best matched the aircraft data at levels where radiosonde and aircraft overlapped. When the aircraft sampled convection far from the radiosonde ships in the Intensive Flux Array (IFA), we had to assume horizontal uniformity over a few hundred kilometers.

c. Quality control procedures

Temperatures and dewpoints were corrected using a ''best guess'' combination of our own interaircraft biases (Table 1) and those determined at the University of California, Irvine (UCI), by Sean Burns [1996, personal communication; UCI P3 average biases summarized in Khelif et al. (1998, manuscript submitted to *J. Atmos. Oceanic Technol.*)]. Altitudes were recomputed to be consistent with the corrected thermodynamics. When possible, we removed heading-related wind biases. Most of the soundings were constructed using the ''original'' aircraft winds, which do not contain the most recent GPS corrections. However, comparisons of hodographs based on the old winds and those corrected using the GPS data using the technique of Matejka and Lewis (1997) suggest that differences will not affect our conclusions. Details appear in the documentation of individual soundings.[3]

Estimated instrumental uncertainties for aircraft measurements are for temperature, 0.1–0.2 K; for dewpoint, 0.5 K; and for sea surface temperature, 0.5 K. These estimates are based on comparison of Table 1 with Burns' table of aircraft biases, which is referenced to measurements from other platforms; and comparison of bulk heat and moisture flux estimates using these measurements to eddy-correlation measurements in comparable conditions. We believe radiosonde data are close to expected accuracies at the heights for which they were used (typically 500–250 mb)—that is, temperatures to within ±0.2 K and relative humidities to within ±3–5%. Relative humidity data are generally considered unreliable above 250 mb (e.g., Lin and Johnson 1996). Most of the wind data in the lowest 6 km are from aircraft. The expected measurement error for aircraft winds are ~±1 m s^{-1}, with measurement error for wind shear about half that, and in some cases as little as ±0.1 m s^{-1} km^{-1}.

In studies like this, representativeness of the measurements is more of a concern than instrumental uncertainty. When there is considerable horizontal variability, we cannot be certain that the constructed sounding represents the ''true'' environment to within instrument uncertainty. Furthermore, the constructed sounding is not

[3] Available via anonymous ftp from NSSL's Mesoscale Research and Applications Division (mrd3@nssl.ucar.edu in the directory pub/TOGA-COARE/coare_coare_sdg_nobias) or from the first (corresponding) author. We used the NSSL-generated dataset, which has dewpoints on both P3s 0.5°C lower than in the UCI dataset. This is because UCI has the ''original'' dataset, whereas the NSSL data were ''corrected'' based on tower flybys after the experiment (Burns 1996, personal communication)—an indication of the difficulty in obtaining accurate data.

TABLE 2. Description of convection for selected TOGA COARE turboprop missions. Convective class (Conv Cls) is from *TOGA COARE at a Glance* (Yuter et al. 1995).

Date	Conv Cls	Description
6 Nov 92	3	Stationary E–W band going stratiform rapidly; new cells on S side; one set of new cells formed NE–SW line, which became scattered cells.
19 Nov 92	2	WEAK convective organization; initial target ENE–WSW weakening convective band; later convection encountered was confirmed to be organized along the outer edges of a cold pool.
26 Nov 92	1	Convection mainly determined by interaction old outflow boundaries, main target moved from 270° at 5 m s^{-1}.
12 Dec 92	3	Main system a squall line with NW–SE (310°–330°) leading edge: moving from 060° at 9 m s^{-1}. E–W (270°–280°) bands W and S of large system, which was evolving toward stratiform. E–W bands too short lived to track.
13 Dec 92	4	Huge precip. system; stratiform dominant. Focus on last half aircraft mission near convective cells and bands on SW flank of big system. Bands 290°–111° ± 30°.
14 Dec 92	4	Widespread convection; randomly oriented.
15 Dec 92	4	Widespread convection, aircraft (and sounding) focus on 2–3 ENE–WSW bands; moving from 330 at 5 m s^{-1}.
9 Jan 93	0 (orig. 1)	Squall line turned E–W arc moving N from 1700–2400 UTC; on satellite images from before 1400 UTC to at least 0600 UTC 10 Jan. Weakening; nearly stationary by 0400 UTC 10 Jan.
16 Jan 93	0 (orig. 1)	First line worked by aircraft was a short-lived E–W line that was active only about 2 h; this coexisted with a series of more persistent (2–4 h +) NNW–SSE lines moving toward 250° at 5–7 m s^{-1}. Details from *Vickers* radar.
17 Jan 93	1	Target is E–W zone of convective bands that rapidly becomes stratiform. Zone stationary; bands move S at ~3 m s^{-1}. A 200-km long N–S appendage curving to NNW–SSE extends south from the line and moves toward west at 3.5 m s^{-1}. E–W zone lasts 2–3 h, appendage at least 8 h. Details from *Vickers* radar.
18 Jan 93	1	Target is broad zone of precip. oriented from 270° to 280°; 3 long N–S lines extending S from zone move westward at 5–6 m s^{-1} on average; E line persisted after others died.
4 Feb 93	2	080°–260° thin, leading convection, trailing stratiform line moving from 180° at 7 m s^{-1}.
6 Feb 93	2	NW–SE rainband on outer reaches of Tropical Cyclone Oliver with short spurs normal to rainband axis. Zipser tracks central portion of rainband from 235° at 2.5 m s^{-1} at 1630–2030 UTC; LeMone gets ~5 m s^{-1} from Electra leading-edge locations at 3 km.
9 Feb 93	3	WNW–ESE line, up to 200-km long. P3 radar shows E end line moves from 200° at 8.5 m s^{-1} at 1600–1700; 6.7 m s^{-1} at 1700–1800; 4.0 m s^{-1} at 1800–1900 UTC. First observed at 1430.
10 Feb 93	1 (orig. 2)	E–W squall line moving from 180° at 11 m s^{-1}; first observed at 1822; studied 2300–2400 UTC.
17 Feb 93	1	Two convectively active E–W lines; northern line moves from 355° at 1.9 m s^{-1} but appears to be growing on the north side. Sounding applies to north of northern line.
18 Feb 93	2	System of stationary E–W lines, which moved southward in discrete jumps. Lines seemed to draw in air from S (i.e., S wind at 30 m stronger near line than in the environmental sounding). See Hildebrand (1998).
20 Feb 93 (S)	2	Horseshoe-shaped squall line with N–S leading edge moving E at 12 m s^{-1}; E–W lines form legs of horseshoe. Southern E–W line observed propagating N into modified air; strong single cell moves E into cold pool at 15 m s^{-1}. This sounding best guess for squall line and lines to S of horseshoe, but looks modified.
20 Feb 93 (N)	2	This sounding environment for E–W line forming on N leg of horseshoe late in pattern.
22 Feb 93	4	Squall line; oriented NNW–SSE with strong N–S segment during bow-echo stage, when there was a vortex at the north end of the squall line and a ''secondary'' transverse band extending rearward from the squall line. Duration at least from 1930 to 2500 UTC.

necessarily the same as when the system was forming. At the highest levels in the sounding (~200–100 mb) vertical smoothing of the radiosonde winds on occasion may have eliminated features observed over large horizontal distances, though we tried to retain the large-scale maximum in the easterlies discussed by Lin and Johnson (1996).

d. Analysis of convective systems

Convective structure and propagation was determined from the lower fuselage radar maps prepared by the NSSL Mesoscale Research and Applications Division and videos of the R/V *Vickers* radar provided by S. Rutledge of Colorado State University. The days examined are summarized in Table 2. More detail on individual days can be obtained on the World Wide Web (Yuter at al. 1995). In examining the radar patterns, we focus on the degree of linear organization of the convection, and its alignment to the environmental wind hodograph. We focus on degree of linear organization because previous work [summarized in LeMone and Moncrieff (1994) and in the introduction] shows that convective organization influences MCS's kinematic fields, which in turn determine the vertical transport of horizontal momentum, the rate of anvil and cold-pool spread, and the properties of the air reaching the surface, which determine surface fluxes. We focus on convective-band orientation because it determines the properties of the vertical transport of horizontal momentum relative to the earth.

Convective-band orientation is averaged over the time the system was sampled. For systems with arc-shaped leading edges, the center of the arc is used to define the

orientation. Convective-band motion is found from the leading-edge envelope, which allows near-continuous propagation even when new cells form at the leading edge. We define line motion as the component of motion normal to the line, even though there can be considerable motion of the cells along the line.

3. Results

a. Shear effects

We sort the convection into five categories: 1) shear-perpendicular, 2) shear-parallel, 3) smaller-scale convection, 4) convection not aligned by the shear, and 5) convection with no apparent organization. Categories 1 and 2 are loose definitions. Shear-perpendicular lines tend to be nearly normal to the shear in the lowest 1–2 km. They are similar to the fast-movers of Barnes and Sieckman (1984) but not necessarily fast moving relative to the ground. According to Alexander and Young (1992), shear-parallel lines are close to parallel to the shear at midlevels, between about 800 and 400 mb. Smaller-scale convective bands are narrower in the cross-line direction and have little stratiform precipitation until they dissipate. Convective bands not aligned to the shear are divided into two subcategories, those organized by cold pools, and those with no obvious organizing mechanism. In the first case, alignment was determined either at the earlier stages of an MCS now in its dissipating stage, or alignment was by the cold pool from a previously existing MCS. We leave bands with no obvious organizing mechanism unclassified. Convection with no apparent organization showed no consistent pattern.

1) SHEAR-PERPENDICULAR LINES

Figures 1–3 show convective bands that are roughly normal to the low-level shear, as defined from 1000 to 800 mb or to the maximum low-level wind, whichever is lower in altitude. Their orientation is compared to that predicted according to shear in fixed layers in Table 3. Shear-perpendicular lines are predicted for low-level shears in excess of 2 m s^{-1} per 100 mb—5 m s^{-1} from 950 to 700 mb for Alexander and Young (1992) or 4 m s^{-1} in the layer from 1000 to 800 mb. If this criterion is satisfied, and if the line orientation is predicted to within 30°, the success of the prediction is designated by boldface lettering.

All the hodographs in Figs. 1–3 exhibit a wind maximum between 850 and 550 mb, and the convective lines propagate at a speed corresponding to the component of the maximum wind, normal to the line, ±2 m s^{-1}, within the certainty of the winds at that level. Numerical simulations by Robe (1996a,b) for idealized shear profiles, Trier et al. (1998) for 22 February in TOGA COARE, and others indicate this to be a common property of such lines, as do the observational results of

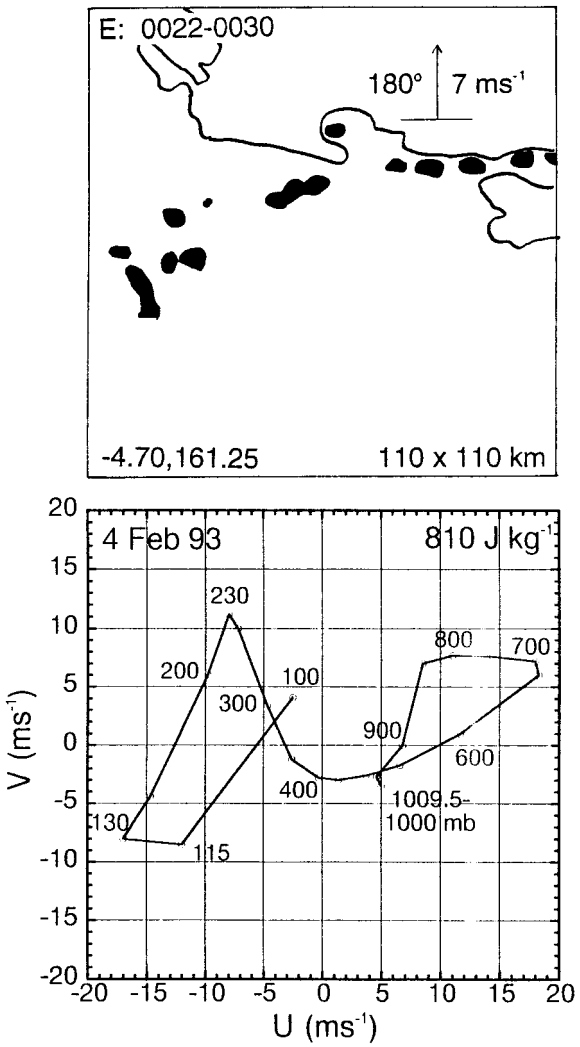

FIG. 1. Shear-perpendicular line (within ~±30° of normal to the vertical shear of the horizontal wind beneath the low-level jet) of 4 February, with environmental wind hodograph. Electra radar (ELDORA) reflectivity pattern at 0.3 km MSL (≥25 dBz shaded, leading edge of 15-dBz echo outlined), over 110 km × 110 km area whose location is indicated by the latitude and longitude of the lower-left corner. Vector shows motion of the convective band, defined as normal to the band. Winds are earth-relative, in a right-handed coordinate system with *U* positive east. Irreversible CAPE based on 50-mb parcel appears at upper right of wind hodograph; aircraft (E: Electra) and times of composite (UTC) appear in upper-left corner of reflectivity map.

Barnes and Sieckman (1984), Jorgensen et al. (1997), and others. The low-level inflow shear is of the right sign for longevity, according to Rotunno et al. (1988, hereafter RKW). Six of the seven lines in Figs. 1–3 fall within Barnes and Sieckman's fast-mover category ($c \geq 7$ m s^{-1}). The system of 6 February, which propagates at 2.5 m s^{-1}, falls within the slow-mover category ($c \leq 3$ m s^{-1}). Inspection of Figs. 1–3 shows that the shear-perpendicular orientation applies ±30° for all but 12 December using the low-level shear below the low-level

TABLE 3. Vector wind difference **ΔV** (expressed as direction/speed dd/ff) through selected layers as criteria for mesoscale linear structure and alignment. Orientation defined to match dd for easy comparison of observed to predicted alignment. For shear-⊥ lines, orientation defined normal to the line, positive in direction of line movement, using the direction from which the line moves. For shear-parallel bands, orientation is defined along-line, with 180° correction as necessary to match dd. If **ΔV** exceeds ''⊥'' threshold, lines should form normal to the low-level shear: if **ΔV** exceeds ''‖'' threshold, lines should form parallel to the midlevel shear. Threshold is 5 m s^{-1} for 950–700-hPa and 800–400-hPa layers (Alexander and Young 1992); threshold is 4 m s^{-1} for 1000–800 hPa. Bold numbers indicate correct prediction of linear structure and alignment (±30°): italics for secondary lines.

		MCS Orientation (°)		Vector wind difference **ΔV**					
				950–700 hPa (⊥?)		800–400 hPa (‖?)		1000–800 hPa (⊥?)	
Day	MCS Classification (Figs. 1–3, 5–9)	Band-⊥ (all primary)	Band-‖ p = primary s = secondary	dd (deg)	ff (m s^{-1})	dd (deg)	ff (m s^{-1})	dd (deg)	ff (m s^{-1})
4 Feb	Shear-⊥	**170–180**		234	16.7	47	15.4	**208**	**12.7**
6 Feb*	Shear-⊥ w/shear ‖ bands	**225–243**	36–57 (s)	**264**	**9.1**	90	0.4	**264**	**9.1**
12 Dec	Shear-⊥ w/shear ‖ bands	060	106 (s)	106	9.9	119	3.1	111	8.4
20 Feb N	Shear-⊥ w/shear ‖ bands	**270**	**80** (s)	238	9.9	***81***	***14.5***	**243**	**9.2**
20 Feb S	Shear-⊥ w/shear ‖ bands	**270**	**80** (s)	**265**	**3.3**	**89**	***12.2***	**256**	**7.8**
22 Feb	Shear-⊥ w/shear ‖ bands	**240–245**	**90** (s)	**236**	**9.7**	***113***	***9.5***	**258**	**12.4**
9 Feb	Shear ‖ and ⊥	**200**	**110 (p)**	134	4.6	**82**	**16.7**	**216**	**6.6**
10 Feb	Shear-‖ (and ⊥?)	170–180	**80–90 (p)**	215	5.5	**66**	**19.2**	219	10.9
6 Nov	Shear-‖		**90 (p)**	112	2.2	**88**	**12.9**	262	2.1
8 Feb	Shear-‖		**90 (p)**	266	4.6	**86**	**7.5**	226	4.3
16 Jan	Mixed, smaller scale	63	**250 (p)**	273	2.1	**260**	**11.8**	0	1.0
17 Jan	Mixed, smaller scale	**90**	**270 (p)**	111	2.8	**242**	**15.0**	**97**	**4.2**
18 Jan	Mixed, smaller scale	**72**		15	5.2	301	17.2	**56**	**4.0**
19 Nov	Forced (old cold pool)	**No preferred orientation**		214	5.0	**271**	**4.0**	**240**	**1.6**
26 Nov	Forced (old cold pool)	No preferred orientation		106	7.4	78	8.6	149	7.1
9 Jan	Forced (old cold pool) + no apparent organization	180–210 assoc. with dissipated squall line		254	3.3	311	5.7	243	0.7
15 Dec	Unclassifiable → shear-⊥	**328**		60	5.9	127	5.8	**348**	**4.0**
17 Feb	Unclassifiable	355		117	4.9	127	1.5	81	4.7
13 Dec	No apparent org.			94	13.0	84	7.7	90	3.0
14 Dec	No apparent org.			158	5.2	68	6.9	201	5.5
GATEF	Shear-⊥('fast')	**70**	160	**71**	**11.5**	158	3.7	**86**	**4.7**
GATES	Shear-‖ ('slow')	300	30	23	4.3	65	4.3	5	2.5

* Secondary lines parallel to low-level (1000–800 mb) shear.

wind maximum. Of the fixed-level shear criteria, the 1000–800-mb shear vector does a better job of predicting line orientation than the 950–700-mb layer used in Alexander and Young. In all cases, the low-level shear exceeds the 2 m s^{-1} per 100-mb threshold.

The shear-perpendicular lines in Figs. 1–3 occur in an environment with westerly winds at low levels and, with the exception of 22 February, strong easterly winds aloft. The low-level vertical zonal shear is positive with the exception of 12 December. All are in the convergent zone of the intraseasonal oscillation (ISO: Madden and Julian 1972) preceding the maximum low-level westerlies (Lin and Johnson 1996). Low-level meridional shear is significant on 4, 9, and 10 February. Consistent with this, all the bands except that of 12 December propagate eastward or northward.

''Secondary'' bands develop in four cases (Fig. 2), either trailing the primary convective band (Fig. 2a) or leading it (Fig. 2b). The occurrence and orientation of the trailing bands parallel to the midlevel shear are correctly predicted (threshold 5 m s^{-1} from 800 to 400 mb or 1.25 m s^{-1} per 100 mb). Studies of the trailing secondary bands of 20 and 22 February indicate that their evolution and alignment are determined by rearward advection of mass and moisture from the environment ahead of the leading-edge squall line. Lewis et al. (1998) demonstrate the structure of the middle east–west band of 20 February in Fig. 2a is, above the lowest levels, strongly tied to the leading squall lines' front-to-rear updraft. The long east–west band of 22 February, marked by an ***A*** in Fig. 2a, formed entirely above the surface-based cold pool on 22 February (Jorgensen et al. 1997; Trier et al. 1996). Trier et al. (1997) use a numerical simulation that evolves similarly to the Jorgensen et al. (1997) observations to describe the evolution of the east–west band. As in Fig. 2a, the simulated 22 February MCS moved at nearly the speed and direction of the 800-mb environmental wind maximum. The air that eventually formed the east–west band originated at low levels ahead of the MCS. It was lifted to heights above the environmental wind maximum and then transported rearward by the system-relative rearward flow. While there was potential for rearward advection at heights above 800 mb along the entire leading

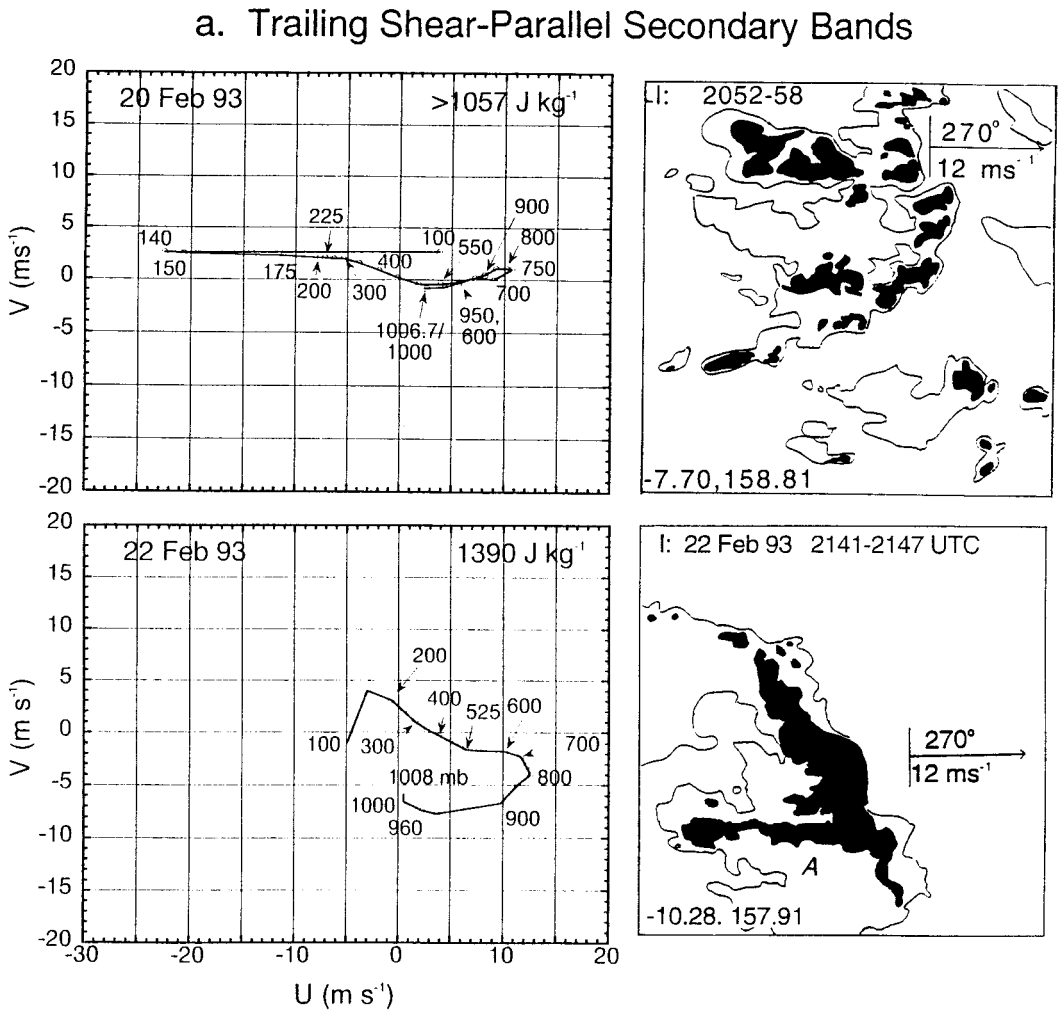

FIG. 2. As in Fig. 1 but for shear-perpendicular lines with secondary bands (a) trailing the primary band and (b) ahead of the primary band. Reflectivity patterns (≥30 dBz shaded; ≥20 dBz outlined) are P3 lower-fuselage radar composites for the time (UTC) and aircraft (H: *NOAA42*, I: *NOAA43*) indicated, over 240 km × 240 km area. Latitude and longitude corresponding to lower-left corner appears there. Motion vectors are for the primary bands. Motion for

edge of this MCS, the southern end had the strongest component of relative front-to-rear flow. This was reinforced with time, first by two-dimensional storm-generated front-to-rear flow and then by front-to-rear flow associated with the southern line-end vortex. Multiple secondary bands occurred in both the observed and modeled MCS.

Trailing bands appear to be a feature of later-stage convection bands with a substantial component of rearward line-normal shear, but are absent if the midlevel shear is parallel to the primary band. Figure 4 shows the 22 February system with no prominent trailing bands, 90 min after the band was first observed in what was believed to be its early stages (Jorgensen et al. 1997). Figure 2a shows the MCS with the trailing band 90 min later—at least 3h into the primary band's lifetime. Similarly, the 20 February system, which has trailing bands and substantial midlevel front-to rear shear (Fig. 2, Table 3), is in a ''late stage'' of evolution (Lewis et al. 1998). Conversely, the relatively simple structure of the 4 and 10 February bands could be related to the small angle between the convective line and the shear at middle levels. The 10 February system was a mature squall line when the P3s first intercepted it at 1823 UTC—nearly five hours before the echo pattern in Fig. 3, allowing ample time for secondary bands to form. Indeed, Hu and Barnes (1994) characterize the 10 February band as shear parallel; and the middle-level shear does a better job of ''predicting'' orientation than does the low-level shear, even if we use the shear from 1000 to 875 mb (Fig. 3, Table 3). Similarly, the remarkable 250-long quasi-two-dimensional radar depiction of the 9 February line that appears in Smull et al. (1996) shows no secondary bands, and represents the system 2.5 h

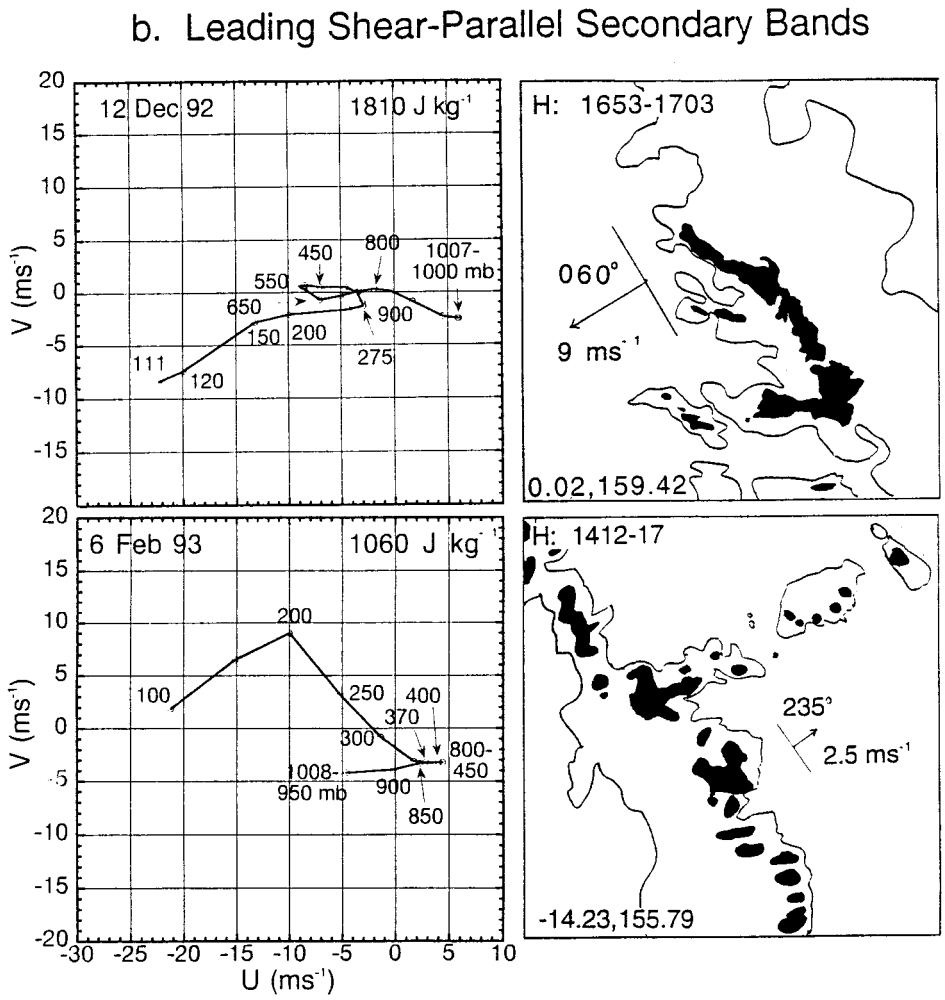

FIG. 2. (*Continued*) trailing secondary bands: 20 February, ~2–2.5 m s^{-1} northward during time of observation; 22 February, motion negligible (Fig. 2, Jorgensen et al. 1997). For leading secondary bands: 6 February bands move SE at ~8–10 m s^{-1} between 14 and 16 UTC; 12 December bands too short lived to track (Table 2).

after it was first detected by the aircraft (Table 2), about a half hour after the reflectivity pattern of Fig. 3.

The secondary bands ahead of main bands in Fig. 2b are more parallel to the *low*-level than the midlevel shear (Table 3). The ''slow'' lines in GATE were also parallel to the low-level shear [4 m s^{-1} between 1 and 3 km from Fig. 9 in Barnes and Sieckman (1984); also see Table 3]. In the case of the 6 February secondary band, which looks like a small squall line moving southeastward at ~8–10 m s^{-1}, this might be a coincidence since the environmental sounding, which focuses on the primary line, may not represent its inflow. The along-shear orientation of the bands is consistent with shear-modified Rayleigh instability (Robe 1996a,b) as described by Asai (1970), or some sort of inertial, inflection-point, or mixed flow instability [see Etling and Brown (1993), and references therein].

2) SHEAR-PARALLEL LINES

Figures 3 and 5 show the convective bands parallel to the shear at middle levels. All four have substantially larger midlevel shear than low-level shear, and all four are aligned to within 30° of the midlevel shear. The occurrence and orientation of all four are predicted by the Alexander–Young criterion (Table 3). Two of these lines, 9 and 10 February, have significant low-level *environmental* shear to support convergence at the leading edge by opposing the vertical shear generated in the cold pool as discussed in RKW. The 18 February line (Fig. 5) develops such shear locally (i.e., strong southerlies near the surface) but not sufficiently to maintain a single, long-lived system. Rather, the first line persisted only 2 h, to be replaced by a second line to the south, which was replaced by a third. Thus, while individual bands remained stationary, the convection

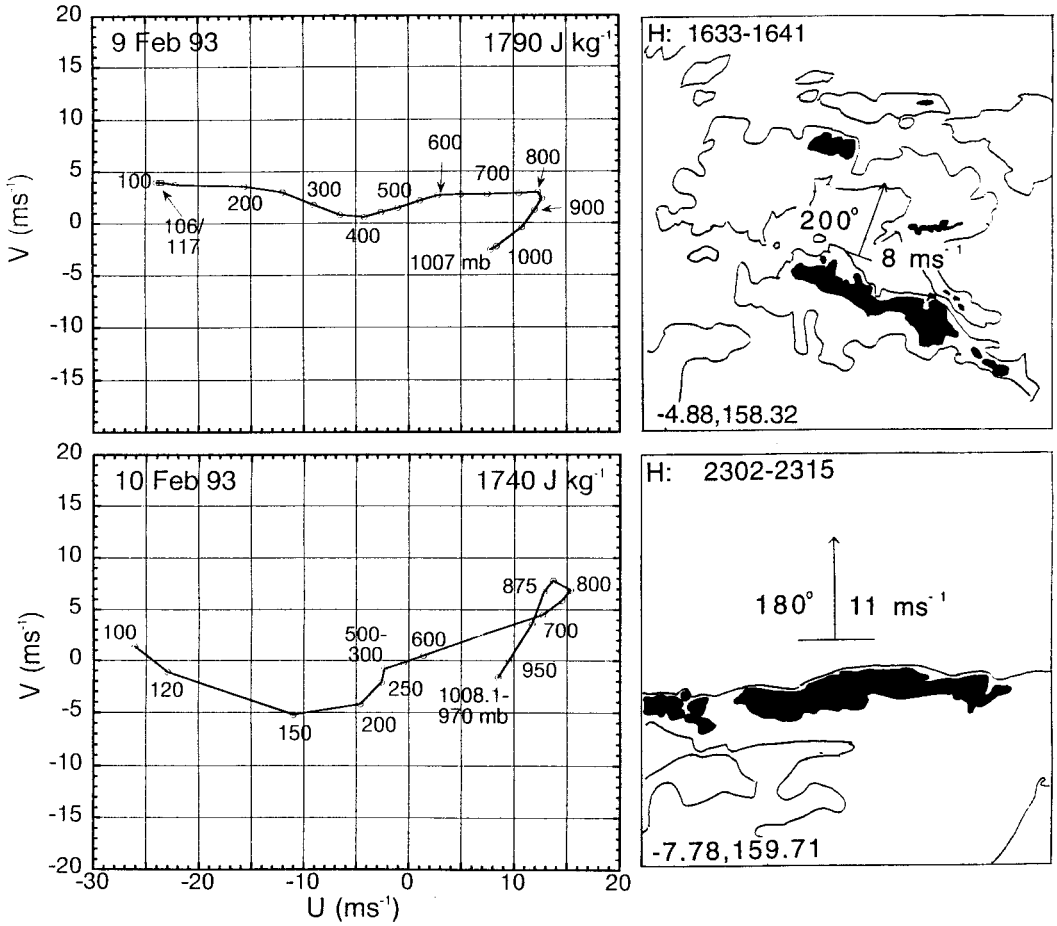

FIG. 3. As in Fig. 2 but for convective bands that are normal to the low-level shear and parallel (±30°) to the midlevel shear (from 800 to 400 mb).

propagated southward in discrete ''jumps'' (Hildebrand et al. 1996; Hildebrand 1998). Portions of the 9 February convective band (Fig. 3) also exhibited some of this jumping behavior, but the leading-edge reflectivity envelope progressed forward smoothly. Several of the shear-parallel lines observed in COARE had short lifetimes (e.g., 6 November, and the secondary lines on 12 December in Fig. 2b; see Table 2).

Like most of the shear-perpendicular bands, the shear-parallel bands occur in environments with west winds near the surface and strong easterly winds aloft, and low-level convergence within the IFA (Lin and Johnson 1996), placing them in the convergent region of the ISO preceding maximum low-level westerlies. The individual bands in Fig. 5 were stationary. The cause(s) of these bands is unknown, although their alignment is consistent with origins similar to those suggested for the leading shear-parallel secondary bands in Fig. 2b.

3) SMALLER-SCALE CONVECTION

This convection [all Class 1, implying area of cloud tops colder than 208 K less than 6000 km^2 (Mapes and Houze 1993)] was mostly relatively shallow with thin echoes (Fig. 6). Since the convective lines sometimes exceed the 100-km length used by Rickenbach and Rutledge (1998) as the upper limit for their sub-MCS class of convection, our ''smaller-scale'' convection does not correspond exactly to their classification.

Although associated with large-scale low-level convergence (Lin and Johnson 1996), this convection differed from other cases by being associated with westerlies aloft and east winds at the surface—clearly the convergent portion of the ISO following the maximum surface easterlies. All three cases have weaker or shallower versions of the jetlike profiles of Figs. 1–3, normal to thin ''shear-perpendicular'' lines having little stratiform precipitation, and propagating westward at speeds within 2 m s^{-1} of the jet-maximum wind speed. For 17 and 18 January (Table 3), the 1000–800-mb shear predicts the occurrence and orientation of these bands; but the wind maximum on 16 January occurs at too low an altitude to be ''picked up'' by the fixed-level criteria. The shear below the wind maximum exceeds the 2 m s^{-1} per 100 mb threshold on this day, but only from 1000 to 950 mb (Fig. 6).

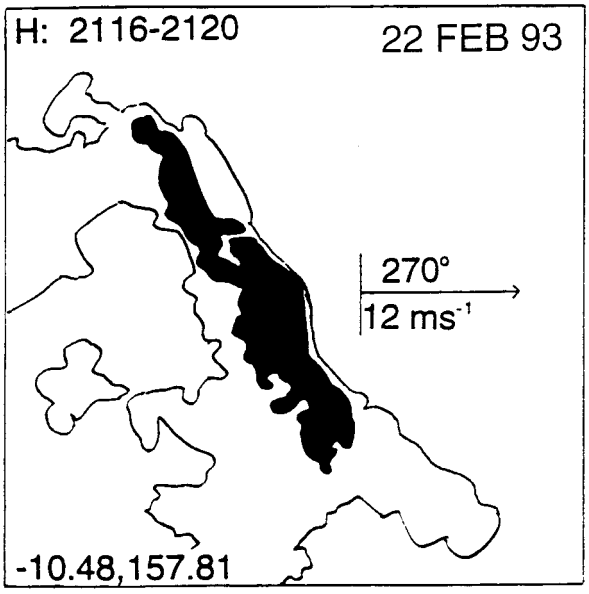

FIG. 4. Reflectivity pattern (≥30 dBz shaded; ≥20 dBz outlined) for 22 February band from 2116 to 2120 UTC lower-fuselage radar composite from *NOAA42*, about 90 minutes before time depicted in Fig. 2, over 240 km × 240 km area.

Rapidly dissipating slower-moving east–west bands also occur on 16 and 17 January; these fit the criteria for shear-parallel lines (Table 3). A longer-lived east–west band lies just to the north of the convection depicted for 18 January. This last band was sufficiently strong to count in one of the other categories, but it probably has different environmental conditions.

The mixed-mode structure of the smaller-scale convection of 16–18 January is reminiscent of convection described by Malkus and Riehl (1964); its size and spacing are like some of the ''fair weather'' cases described in LeMone and Meitin (1981). Such convection has been explained with some success with ''dry dynamics,'' for example, by Sun (1978), in a study of Rayleigh and shear-instability modes, and by Clark et al. (1986) and Balaji et al. (1993), who showed that boundary layer convection could be modulated by tropospheric gravity waves generated by boundary layer convection. These mechanisms compete with cold-pool forcing to produce complex but still patternform convection.

4) CONVECTION NOT ALIGNED BY SHEAR

Aligned by cold pools. The structure of the convection in Fig. 7 is determined by the cold pool or interacting cold pools from late-stage or dissipated MCSs. For example, the 9 January band is a dying squall line whose history can be traced back at least 10 h (Table 2), when its orientation was probably determined by a shear profile different from that in Fig. 7; indeed, there is subsidence in the IFA (Lin and Johnson 1996). The locally produced convection north of the dying band occurs in isolated small cells or short arcuate bands—convection consistent with small low-level shear in the hodograph (e.g., Chisholm and Renick 1972). Similarly, the convective patterns of 19 and 26 November form along the boundaries of moving and spreading cold pools, but with little preferred orientation. Shear-based criteria do a poor job of predicting organization or alignment: from Table 3, 19 November should have shear-perpendicular bands, and 26 November and 9 January should have shear-parallel bands.

Unclassified convection. We did not classify convection that had linear structure but no obvious relationship to the environmental wind hodograph. Figure 8 shows two examples, the convective bands of 15 December and 17 February. The 17 February band had multiple coexisting lines that appeared to be growing on the north side but drifting southward. This unusual behavior separates this case from the ''smaller scale'' convection that appeared to be aligned by, and to move/grow down the shear through a shallow layer near the surface. On 15 December, the occurrence and alignment of convective bands is correctly predicted by the shear-perpendicular criteria (Table 3), but the band does not move with the lower-level wind maximum (Fig. 8). Rather, one line dominates at a given time as the system propagates in discrete jumps to the southeast, reminiscent of the jumps of the 18 February shear-parallel lines documented by Hildebrand (1998). Neither of these cases has substantial shear at either low or middle levels [although the line(s) on 15 December appear to generate low-level shear locally]. This convection, as in the majority of cases, was associated with the low-level westerlies, upper-level easterlies, and low-level convergence (Lin and Johnson 1996) that precede the maximum westerlies in the ISO.

5) NO APPARENT ORGANIZATION

In this case, radar images revealed no consistent organization. Two examples appear in Fig. 9. We might expect lack of organization in the absence of shear, but there is appreciable low-level shear on 14 December. Since convection is so widespread on these days, old cold pools or other forms of forcing (e.g., gravity waves) could interfere with convective organization.

6) SOME CONCLUSIONS

The best criteria for prediction of linearity and orientation of shear-perpendicular bands included the 1000-mb winds and allowed for a low-level wind maximum below 800 mb. The prediction is best early in the life cycle. The worst orientation predictions were for 12 December (described as ''going stratiform'' in Table 2) and 10 February, which was an impressive system 5 h before the sounding and reflectivity pattern in Fig. 3. Figures 2 and 4 show small orientation changes for the

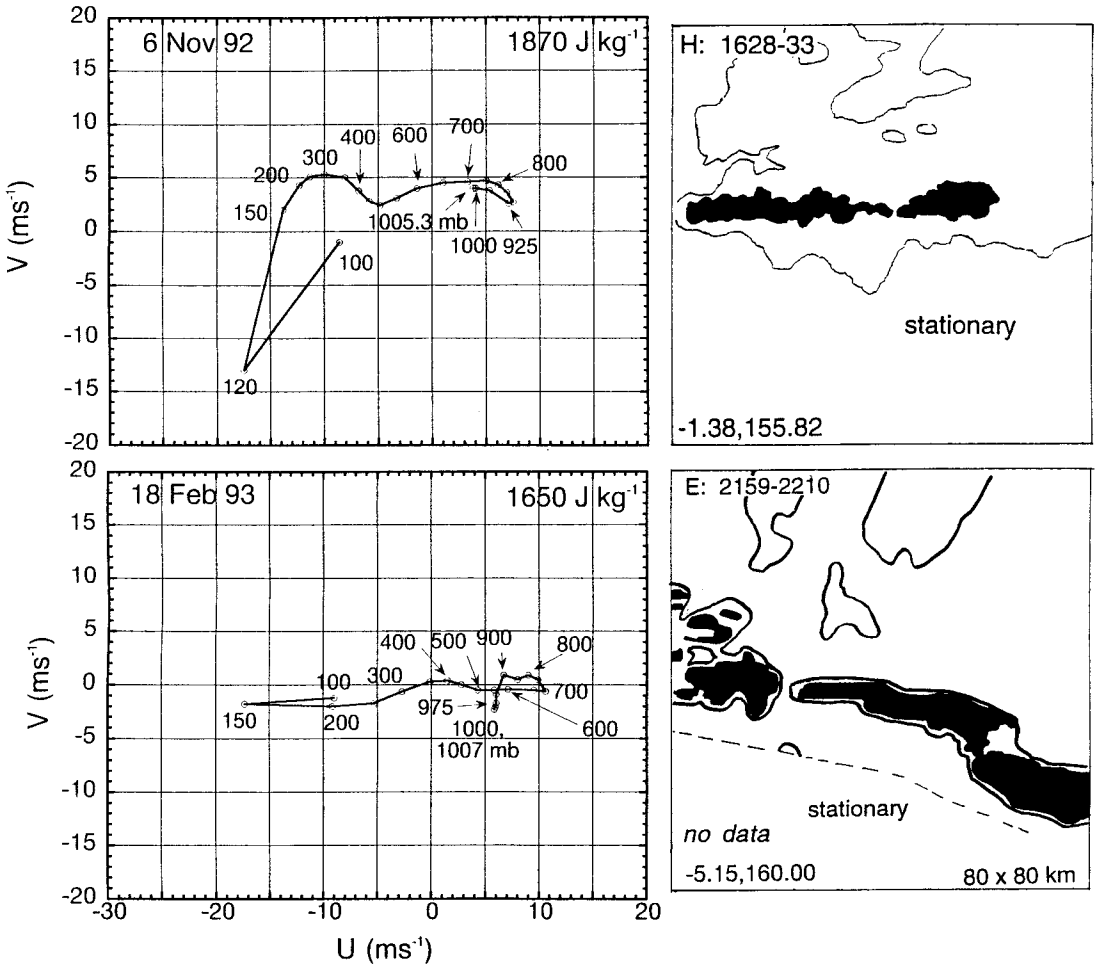

FIG. 5. As in Fig. 2 but for convective bands parallel to midlevel shear. The 18 February radar figure based on ELDORA reflectivity at 0.3 km MSL; reflectivity ≥30 dBz shaded; ≥20 dBz outlined. Area of Electra figure is 80 km × 80 km. Location of lower-left corner indicated by latitude and longitude.

22 February system; it tended to become oriented more NW–SE with time. The orientation of the dying 9 January squall line has no clear relationship to the hodograph in Fig. 7. However, active convective bands can reorient themselves relative to local environmental vertical shear, as noted by Keenan and Carbone (1992) and Halverson et al. (1996). Still, from Table 3, all of the active shear-perpendicular bands fit one criterion: a strong component of low-level band-normal shear. Since these bands travel with the speed of the low-level wind maximum, the low-level band-normal shear beneath the wind maximum varies with horizontal mass flux. *Thus, whether exactly shear perpendicular or not, there is strong mass flux into these lines from the front.*

Trailing secondary bands occur in late-stage shear-perpendicular convection with a substantial rearward line-normal environmental wind-shear component at middle levels, as was the case for 20 and 22 February. In contrast, the systems observed on 9 and 10 February, which were parallel to the midlevel shear, remained quasi two-dimensional through their lives. There is an exception to this pattern: the midlevel criterion predicts NE–SW secondary bands for 4 February that are not observed. However, Fig. 1 covers only one-fourth the area of the other figures and could represent the line early in its evolution, before secondary bands form. This suggests that

1) sufficiently large low-level shear determines the alignment of primary bands and
2) the midlevel shear determines primary-band alignment for subcritical low-level shears.

When both low- and midlevel shears are sufficiently large,

3) convective bands whose alignment is predicted by both low- and midlevel criteria remain linear through their life cycles and
4) if the midlevel shear has a significant rearward com-

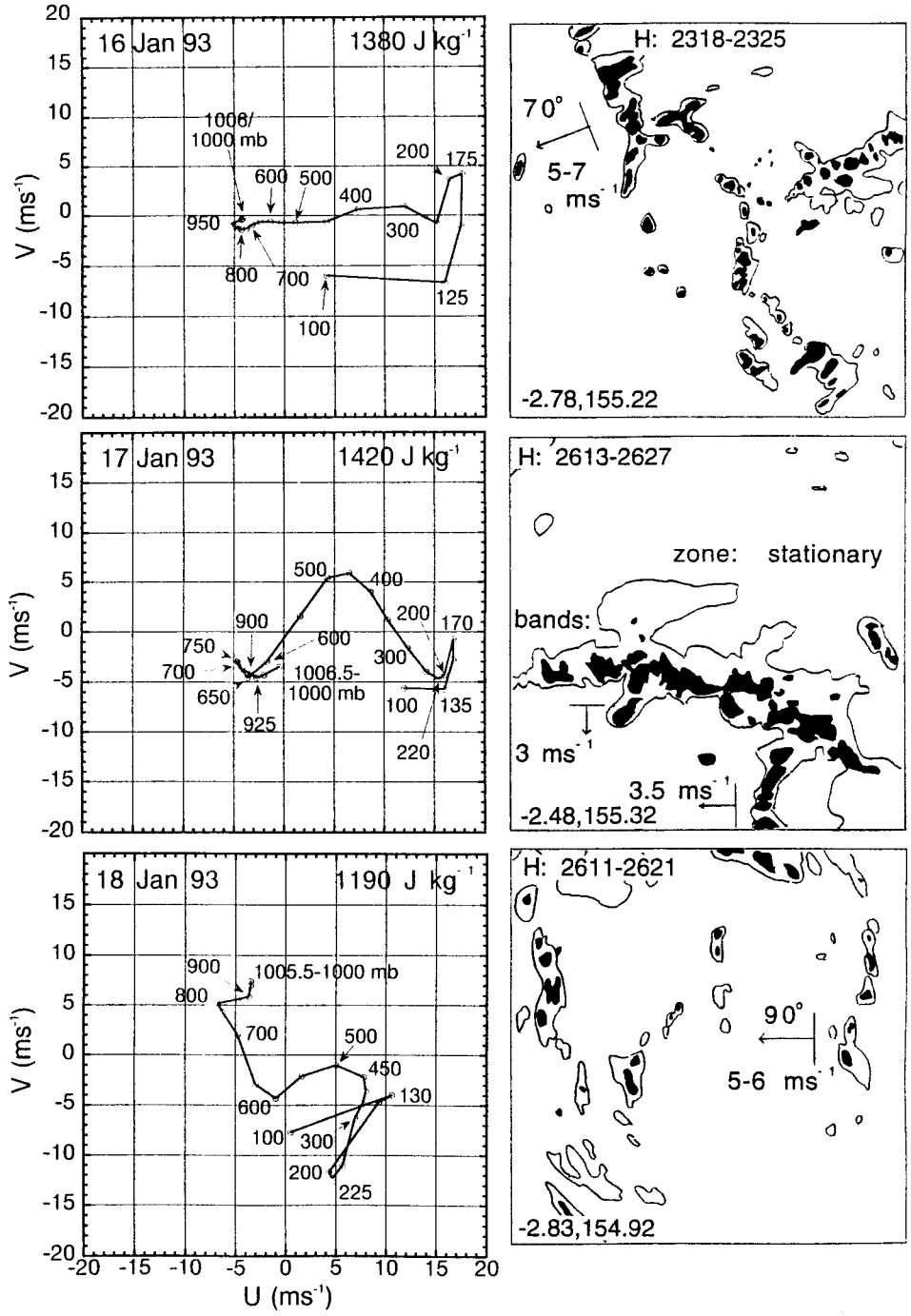

FIG. 6. As in Fig. 2 but for ''smaller-scale'' convection. The roughly east–west bands of 16 and 17 January match criteria for shear-parallel lines; the roughly north–south bands of 17 and 18 January match criteria for shear-perpendicular lines (Table 3).

ponent, secondary bands parallel to the midlevel shear will form behind the primary band. These secondary bands form after the primary bands.

Most of the observed systems occur in the phase of the ISO associated with upward vertical velocities and positive zonal wind and shear at the lowest levels. Meridional wind and shear can be significant. Consistent with this, the convective bands propagate in all directions, with 80% having a motion component toward the east. This suggests that the westward cloud-cluster mo-

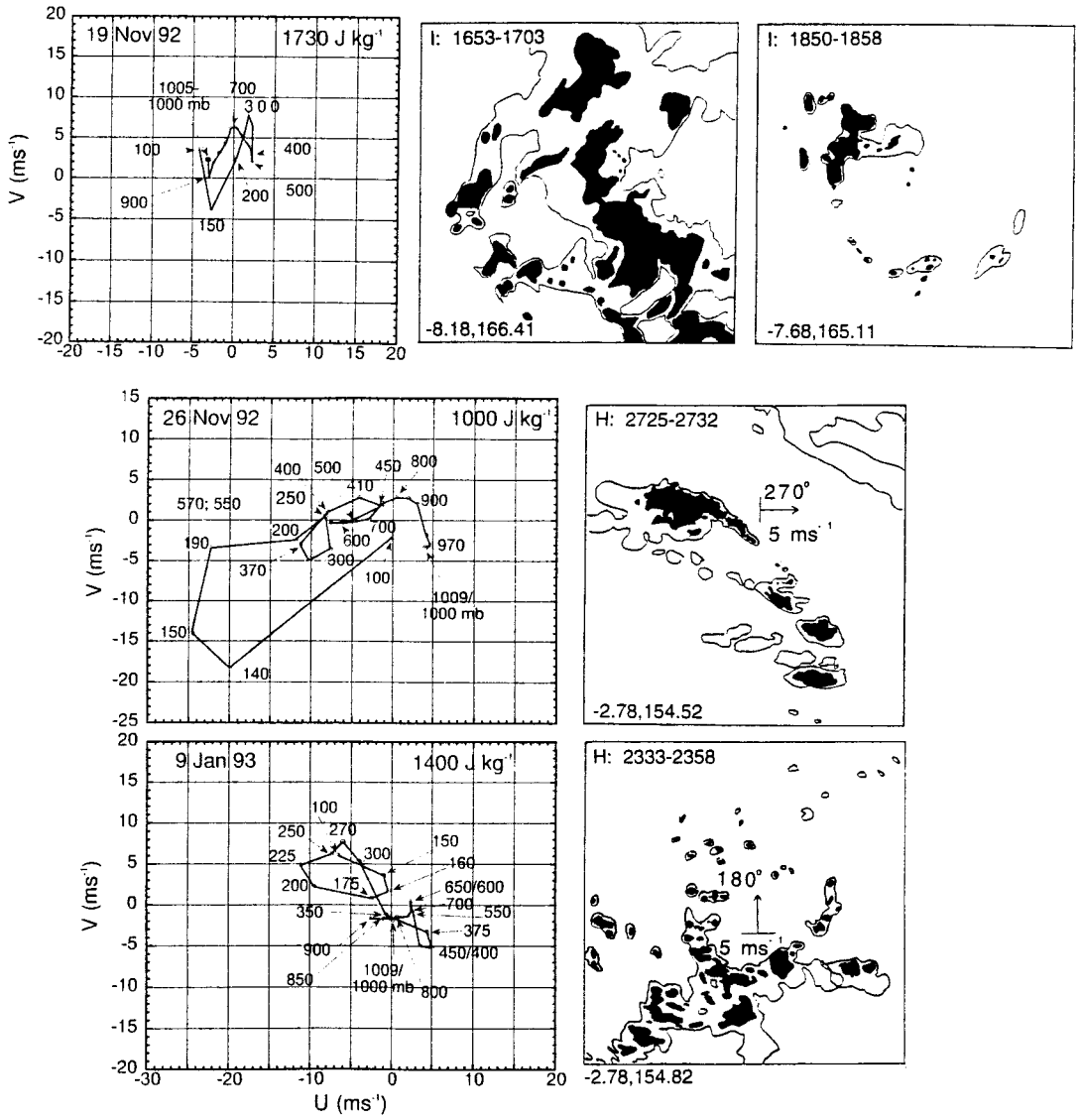

FIG. 7. As in Fig. 2 but for convection with alignment determined by outflow boundaries of dissipating convection or cold pools left after convection dissipated.

tion seen in satellite infrared images (e.g., Nakazawa 1988) is not due to convective-band propagation. The apparent westward motion could result from new convection forming to the west of old convection or, as implied by the strong upper-level easterlies in the wind hodographs, western advection of anvil cloud. Geldmeier and Barnes (1997) note a similar mismatch between convective and anvil motions for a second TOGA COARE system sampled on 10 February 1997. This was also true for the tropical Atlantic during GATE: the satellite cloud tracks of Martin and Shreiner (1981) indicate mostly westward motion, while less than half the convective bands tracked using radar images by Barnes and Sieckman (1984) and LeMone et al. (1984b) move westward.

b. Thermodynamic environment

The average equivalent potential temperature ($\overline{\theta_e}$) profile[4] for the 20 COARE cases in Table 2 appear in Fig. 10, along with the composite soundings for the GATE fast and slow lines from Barnes and Sieckman (1984). COARE θ_e exceed those for the GATE systems to above 200 mb. The difference is almost certainly related to differences in SST. The average SST for the

[4] Calculated from the NCAR/Atmospheric Technology Division (ATD) routine SUDS using the equations of Bolton (1980), for which CAPE and θ_e assume an irreversible (pseudoadiabatic) process.

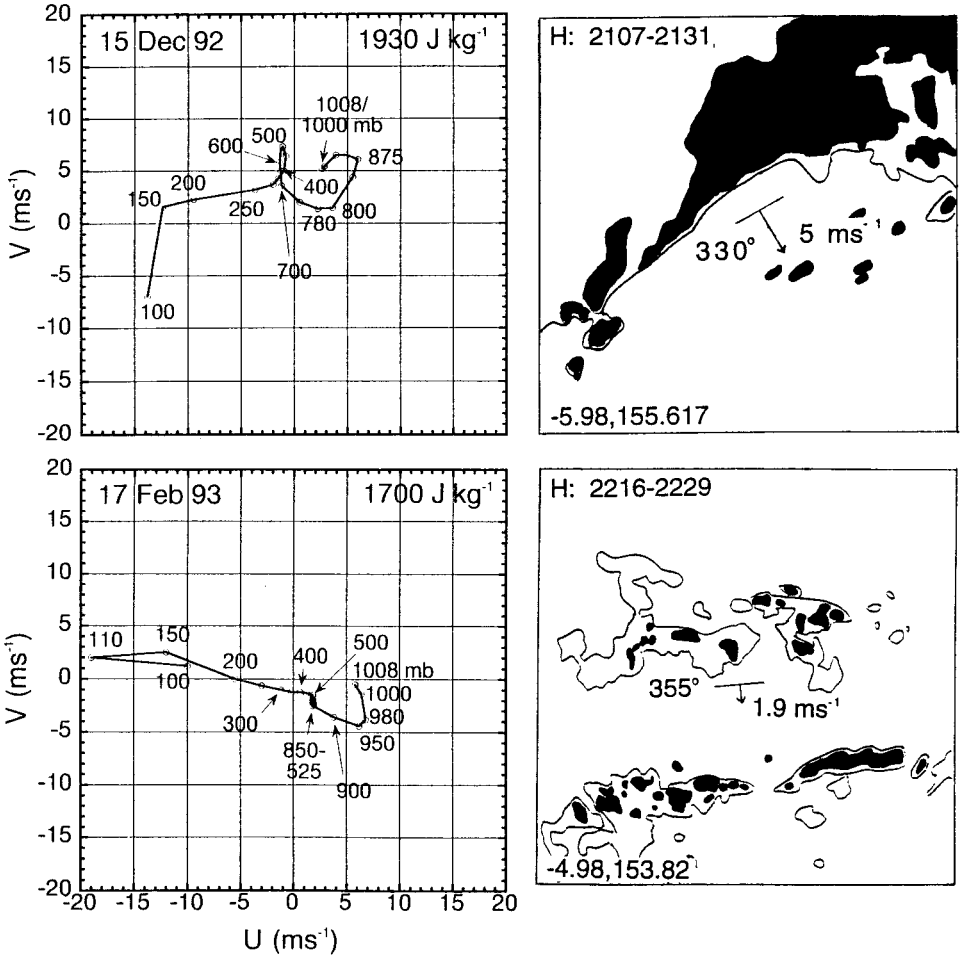

FIG. 8. As in Fig. 2 but for linear convection with alignment not clearly related to the hodograph.

COARE soundings is 29.1°C,[5] significantly higher than the ~27°–28°C for GATE (e.g., Nicholls et al. 1982; Krishnamurti et al. 1976). The vertical gradient of θ_e in COARE is comparable to that for the GATE fast lines, with a minimum between 600 and 700 mb that is 17–18 K less than the surface value.

Within the mixed layer, environmental boundary layer profiles of specific humidity q, θ and θ_e in Fig. 11 closely resemble fair-weather profiles documented elsewhere [trade winds: Malkus (1958), GATE: Nicholls and LeMone (1980) and Fitzjarrald and Garstang (1981), COARE: Dickey (1996)]. This is not surprising since environmental air was defined as undisturbed. The peaks in the frequency distribution, linearly extrapolated to the surface, fall at $q \sim 18$ g kg^{-1}, $\theta \sim 301$ K, and $\theta_e \sim 355$ K. For comparison, the average of the Barnes and Sieckman GATE convection composites are 17.1 g kg^{-1} for specific humidity, 298.5 K for θ, and 348.8 K for θ_e, if we average through the structure[6] in the lower boundary layer. Again, differences are consistent with the differences in SST. The average depth of the mixed layer (h in Table 4) is less than the LCL, the smallest differences being for the soundings based on low-level data collected just ahead of the convective system.

Table 4 summarizes various thermodynamic parameters for the soundings. Immediately obvious are the higher CAPEs for the COARE cases; this is largely because CAPE is strongly related to the higher equilibrium-level altitudes for COARE. The equilibrium level minus level of free convection and CAPE for entries in the table have a linear correlation coefficient $R = 0.74$. CAPE_{500}, the integrated buoyancy between the LFC and 500 mb, should be related to the intensity of convection at that level. It averages about the same as for GATE,

[5] Assuming altitude-corrected *NOAA-43* values, which give reasonable fluxes, are correct.

[6] Structure could be related to launch procedure, since the curves look similar to the COARE soundings before correction using the algorithm of Cole and Miller (1995). Also, soundings are smoothed over 25-mb intervals (G. Barnes 1997, personal communication).

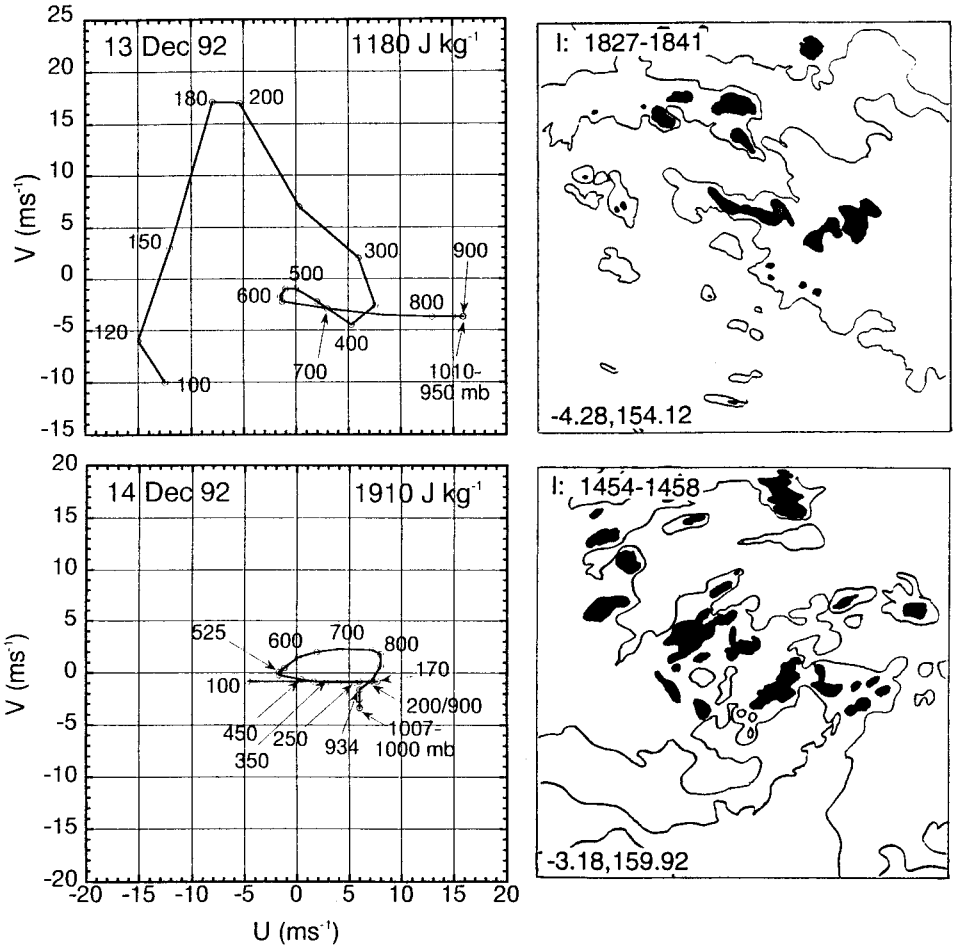

FIG. 9. As in Fig. 2 but for convection with no apparent organization.

but there are days with significantly higher values (14 Dec, 22 Feb). Undilute parcel buoyancies in both cases rarely exceed 3–5 K. Convective inhibition (CIN) is small for the environmental soundings. In this respect, the environmental soundings differ from fair-weather soundings in COARE, which tend to have stronger CIN (soundings in Lucas and Zipser 1996), especially when there are dry air intrusions (e.g., Mapes and Zuidema 1996).

Figure 12 compares the relative humidity profiles[4] for the 20 COARE soundings to those for the GATE slow and fast lines. The relative humidities are slightly higher for GATE at the lowest levels, and lower for GATE above 500–400 mb. The GATE slow-line profile is quite distinct, with relative humidities greater than 80% up to 600 mb.

4. Discussion

a. Modification of soundings by the convective bands

Aircraft data just ahead of the leading edge of several of the slow-moving lines reveal line-normal vertical shear stronger than that for the inflow environmental sounding, with stronger motion toward the line at the lowest levels. Figure 13 shows this behavior for 16 January and 18 February. The 16 January case had significant shear in band-normal wind just ahead (west) of the NNW–SSE band (corresponding roughly to that portion of the band (more solid at the sounding time) just southeast of the ''m s^{-1}'' symbol in Fig. 6, top], while the 18 February east–west band (Fig. 5) had significant band-normal shear just to the south of its leading edge. We also found enhanced shears in aircraft soundings near leading edges on 26 November (just northeast of the largest echo in Fig. 7), 15 December, and 6 February. We did not observe shear enhancement on other days, but it could have occurred.

This behavior should not be as pronounced for the fast-moving lines since the air feeding the system has less time to respond to the line-generated pressure gradient. Consider the simplified line-normal momentum equation in a line-relative coordinate system with x positive in the direction of line motion:

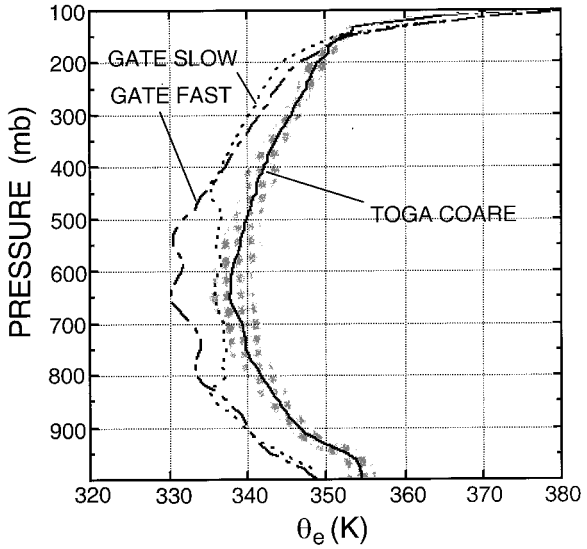

FIG. 10. Average profile of equivalent potential temperature θ_e for the 20 deep convection environments of Table 2. Area shaded inside $\pm\sigma_{\theta_e}$, where σ is standard deviation. The θ_e profiles for the environment of the fast and slow lines in GATE are shown for comparison. GATE data from Barnes and Sieckman (1984). Note soundings do not extend below 1000 mb.

$$\frac{dU}{dt} = \frac{dU}{dx}\frac{dx}{dt} = U\frac{dU}{dx} \sim -\frac{1}{\rho}\frac{\partial p}{\partial x},$$

where dU/dt is the acceleration and $\rho^{-1}\partial p/\partial x$ the pressure gradient felt by air flowing from the environment (e) to the leading edge (le). Integrating and neglecting horizontal variation of ρ yields

$$\frac{\rho}{2}(U_{le}^2 - U_e^2) = P_e - P_{le}. \quad (1)$$

For a given pressure change, it follows that the change in U will be largest for the smallest values of U_e, which is generally associated with smaller propagation speeds. [For example, for 18 February (Fig. 13) but with the environmental wind at the surface $U_e(z = 0) = 0$, the pressure change is ~20 Pa.] This behavior is consistent with the low-level cross sections in Fig. 1 of Barnes and Sieckman (1984), which show a slight increase of mixed-layer U into the slow lines, but virtually no horizontal changes in mixed-layer U ahead of the fast lines. Low-level flow converging beneath growing mesoscale bands is a common observation. The squall-like circulation generated by the tilted heat source in Pandya and Durran (1996) included low-level acceleration of the inflow.

The numerical simulation of the 22 February system by Trier et al. (1996) produces little modification of the inflow boundary layer, but there is warming ahead of the system at middle levels. This implies that the observed environmental sounding may have been similarly modified. That the simulation was so successful at reproducing the observed MCS structure

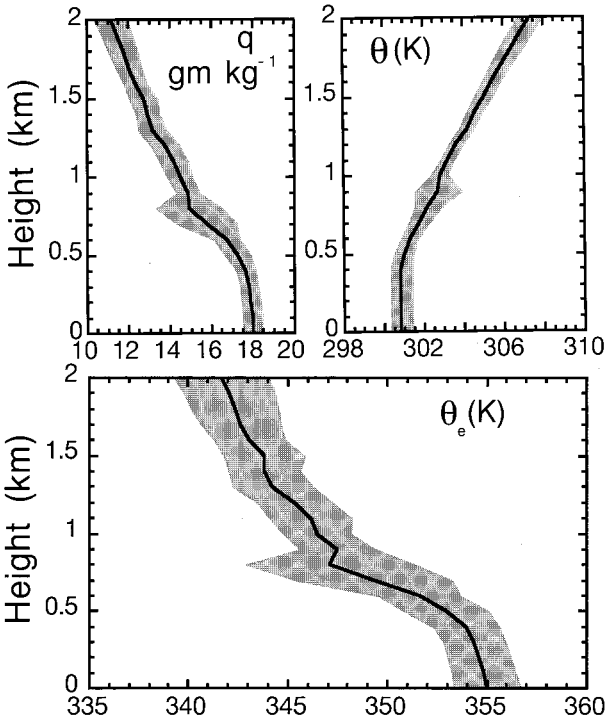

FIG. 11. For lowest 2 km, specific humidity q, potential temperature θ, and equivalent potential temperature θ_e for all soundings in Table 2 except for the southern sounding of 20 February, which had a modified boundary layer. Area inside $\pm\sigma$ shaded.

in spite of potential problems in the environmental sounding may be due to the demonstrated sensitivity of convective-band evolution to conditions at the lowest levels (e.g., RKW). The simulation using the wind profile for the 9 February convective band also produced its general characteristics (Skamarock et al. 1996).

b. Comparisons to GATE convection

1) FREQUENCY OF LINEAR SYSTEMS

A larger fraction of COARE MCSs have poorly organized convection compared to GATE. A third of the mesoscale convection documented by Rickenbach and Rutledge (1998) was not organized into lines. This is roughly the fraction of aircraft-targeted systems that were not organized into lines (Table 3), if we include the convection likely organized by antecedent cold pools. During GATE, the impression of both shipboard (R. A. Houze 1996, personal communication) and airborne observers (including two of the authors, Zipser and LeMone) was that most of the convection was organized in linear patterns. A perusal of the *GATE International Meteorological Radar Atlas* (Arkell and Hudlow 1977) suggests that the fraction of mesoscale convective systems without orga-

TABLE 4. Thermodynamics of the environmental soundings for COARE convective systems and for GATE fast and slow lines (Barnes and Sieckman 1984). $CAPE_{500}$ is buoyancy integrated from the level of free convection to 500 hPa. Pressures (P) listed are for minimum environmental Θ_e, and at the surface (SFC), lifting condensation level LFC, and parcel equilibrium level (EL). z_{LCL} and h are height of the LCL and the depth of the mixed layer.

	CAPE ($J\ kg^{-1}$)	CIN ($J\ kg^{-1}$)	$CAPE_{500}$ ($J\ kg^{-1}$)	Θ_e(sfc) (K)	Θ_{emin} (P) (K,hPa)	P_{SFC} (hPa)	P_{LCL} (hPa)	P_{LFC} (hPa)	P_{EL} (hPa)	z_{LCL} (m)	h (m)
6 Nov	1867	−2	399	356	338 (700)	1005.3	936	912	125	631	490
19 Nov	1732	−5	343	356	335 (600)	1005.0	925	903	137	734	592
26 Nov	1004	−18	342	351	337 (600)	1009.0	942	872	158	606	440
12 Dec	1874	−5	414	356	333 (550)	1007.0	942	899	115	591	424
13 Dec	1184	−6	319	353	338 (600–700)	1010.0	921	881	131	814	730
14 Dec	1909	−2	430	357	338 (500–600)	1007.0	925	909	150	752	610
15 Dec	1925	−4	377	358	334 (600)	1008.0	941	909	105	609	433
9 Jan	1399	−5	396	355	335 (400, 700)	1009.0	929	904	142	731	580
16 Jan	1375	−9	272	356	335 (550)	1006.0	935	886	151	650	415
17 Jan	1424	−9	338	357	338 (650)	1006.5	935	895	146	652	512
18 Jan	1188	−7	351	356	340 (550)	1005.5	936	911	124	633	411
4 Feb	812	−6	153	352	327 (650)	1009.5	921	860	144	810	725
6 Feb	1064	−10	303	353	340 (650)	1008.0	935	882	145	664	524
9 Feb[b]	1789	0	413	356	340 (615)	1007.0	945	939	117	559	502
10 Feb	1741	−12	401	356	335 (670)	1008.1	949	885	135	534	342
17 Feb	1702	−7	393	354	338 (650)	1008.0	934	909	130	612	433
18 Feb	1647	−3	373	357	337 (650)	1007.0	938	920	135	631	609
20 Feb N	1332	−16	356	353	339 (725)	1008.0	939	879	139	616	524
20 Feb S[c]	1057	−25	279	352	340 (600)	1006.7	920	843	146	795	747
22 Feb[b]	1386	−1	436	356	339 (600–800)	1008.0	955	941	128	481	435
GATE slow	1138	−3	379	349	335 (825)	1011.8	950	930	170	554	
GATE fast	954	−2	377	349	330 (650)	1012.7	959	941	195	482	

[a] From NGAR/ATD SUDS program, based on Bolton (1980); air parcel 50 mb deep.
[b] Soundings based on data right at leading edge.
[c] This sounding in modified air to the south of squall line system.

nized bands is of the order of 10% or less.[7] The relative paucity of nonlinear MCSs in GATE is probably related to the strong vertical shear associated with easterly waves and the African monsoon flows (Reed et al. 1977). In contrast, days with small vertical shear were not uncommon (Lin and Johnson 1996).

2) FREQUENCY OF SLOW- AND FAST-MOVING (SQUALL) LINES

Of the linear systems, slow-moving convective bands were much more common in GATE than squall lines, which we define, following Barnes and Sieckman, as convective lines moving at speeds $\geq 7\ m\ s^{-1}$. During the 100 days of GATE, only six squall lines were observed, either by radars and aircraft in the B-Scale Array (centered at 8°N, 23°W), or intercepted by aircraft on the ferry from the western tip of Africa (15°N, 23°W).[8] In contrast, Houze and Cheng (1977) report 85 nonsquall (non-fast-moving) echoes with areas greater than $10^3\ km^2$ within ~250 km of the *Oceanographer* radar. Most of these were linear (R. A. Houze 1996, personal communication). Pestaina-Haynes and Austin (1976) document 50 GATE lines within ~220 km of the *Quadra* radar. An average speed of $2.9\ m\ s^{-1}$ implies that most of these lines were slow moving.

In COARE, the frequency of squall lines is greater than for GATE; and they seem to make up a larger fraction of the linear convection. This conclusion is based on examining the *Vickers* radar video. The radar scans out to ~250 km, covering an area comparable

[7] Certainly some caution should be taken in interpreting these fractions, because they were determined by different people, but the *relative* frequency of convection lacking linear organization in the two experiments should hold up to more careful scrutiny. A more important question is whether this relative frequency is true for other time periods.

[8] However, squall or fast-moving lines were disproportionately well documented in the GATE literature. To illustrate, we provide a partial list of GATE papers published on fast-moving lines and a list of *all* the published studies of slow-moving lines known to us. For fast-moving lines: 28 June (day 179), by Houze and Rappaport (1984); 9 August (day 221), by Wei and Houze (1987); 13 August (day 225), by Zipser (1977); 4–5 September (day 247), by Houze (1977); 11 September (day 254), by Leary and Houze (1979a,b) and Gamache and Houze (1985); and September 12 (day 255), documented by Gamache and Houze (1982, 1983, 1985), Leary and Houze (1979a,b), and Johnson and Nicholls (1983). For slow-moving lines: Zipser et al. (1981, hereafter ZML), LeMone (1983), and the modeling study of Dudhia and Moncrieff (1987).

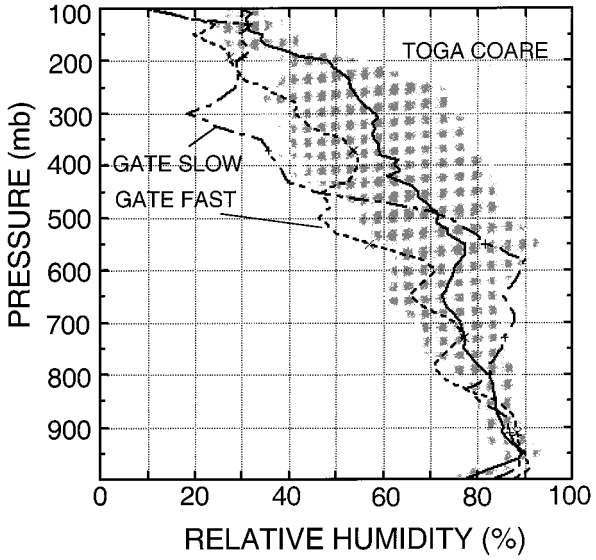

FIG. 12. As in Fig. 10 but for relative humidity, RH. Area shaded inside $\pm\sigma_{rh}$. Individual sounding relative humidities based on Bolton (1980) formula for dewpoints greater than -30°C. GATE data from Barnes and Sieckman (1984).

to the GATE radars. We looked for fast-moving lines; many of these were leading-line-trailing stratiform (LL/TS) systems, as described by Houze et al. (1990). Based on our examination, the radar showed LL/TS squalls[9] on 24 November, several times during the 20–26 December period, around 9–10 January, 30–31 January [31 January squall line in Fig. 5 of Rickenbach and Rutledge (1998)], 9–11 February [11 February systems discussed in Halverson et al. (1996)], and 14–15 February. In contrast, only six squall lines were observed in the GATE B-scale array over a comparable time period. This brief analysis is confirmed by T. Rickenback (1996, personal communication), who notes that propagating squall lines were much more common than slow-moving or stationary lines. This is consistent with the relatively large amount of stratiform precipitation associated with the linear mesoscale convection in Rickenbach and Rutledge (1998). The aircraft cases cannot be used to estimate absolute frequency for squall lines because they represent a biased sample, but we can confirm a greater *fraction* of lines oriented normal to the low-level shear in COARE (seven in Figs. 1–3, six of which were fast-movers or squall lines vs 19 systems examined).

The previously cited studies indicate that GATE squall lines were strong and persistent. They formed normal to the shear beneath the African easterly jet, and moved with its wind maximum westward at 11–14 m s^{-1} (LeMone et al. 1984b). No COARE lines observed by aircraft matched these propagation speeds, and the shear-perpendicular bands of 4 and 6 February certainly did not match their horizontal extent. However, the 31 January 1993 squall line documented in Rickenbach and Rutledge (1998) moved eastward at 15–18 m s^{-1}. There is no mention of secondary bands in the GATE literature. With the notable exception of Leary's work (e.g., Leary 1984), the focus is on simpler systems, depicted as being quasi-two-dimensional. Zipser et al. (1983) document secondary convection in the anvil region of a GATE squall line, and suggest that it is tied to moisture brought back from the leading edge, as in the case of 20 February (Lewis et al. 1998) and 22 February (Jorgensen et al. 1997; Trier et al. 1997) in COARE.

3) LONGEVITY OF SLOW-MOVING LINES

Slow-moving convective bands were common in both COARE and GATE, though not all were parallel to the shear between 800 and 400 mb as in EMEX (Alexander and Young 1992). In GATE, slow-moving bands propagated continuously and persisted for several hours. The 4–5-h lifetime for the slow-moving band of 14 September 1974 (day 257) in ZML is typical; the 7.5-h lifetimes quoted in Pestaina-Haynes and Austin (1976) probably reflect inclusion of the stratiform precipitation that lingered after the convection died out. In contrast, several of the slow-moving bands in TOGA COARE seemed to have shorter lifetimes, and some propagated discontinuously (e.g., 15 December, 18 February).

In this section we examine the factors that could account for the persistence of two well-documented GATE slow-moving lines, those of day 257 (ZML) and day 217 (5 August, LeMone et al. 1984b), and apply the results to COARE slow-moving lines. These factors are a weak cold pool, small convective inhibition, and high lower-tropospheric relative humidities.

Aircraft penetrations (Fig. 14) reveal that the cold pools on both days were shallow and weak. We estimate 300 m as the top of the cold pool on day 257 because the aircraft at 300 m encountered warm air after penetration of the cold-outflow density-current ''head'' and before encountering rain, and we saw no evidence of cold-pool penetration at 610 m. Since the cold pool was ahead of the rain during several penetrations, estimation of the temperature deficit was not affected by wetting. Similarly, there was no evidence of a cold pool at 600 m on day 217; however, we could estimate the temperature drop at 230 m only due to wetting of the temperature sensor by rain.

For system longevity, these weak cold pools must

[9] We equated LL/TS lines with substantial trailing stratiform precipitation as squalls to ease identification during a quick perusal of the radar, since lines thus identified should travel faster than our 7 m s^{-1} threshold for squall lines. However, lines with little stratiform area would be missed.

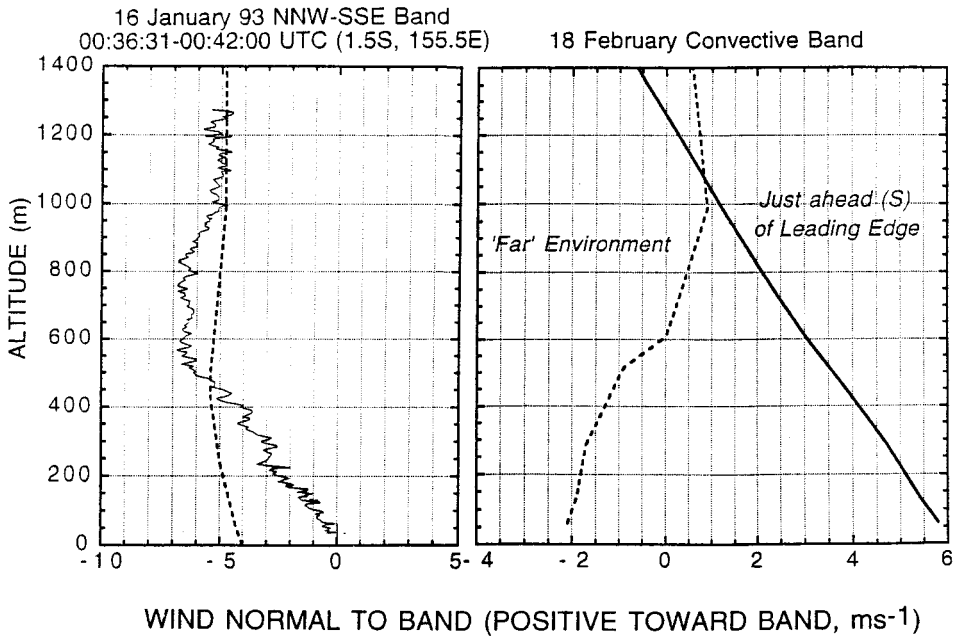

FIG. 13. Evidence of modification of the line-normal wind in the environment just ahead of two convective bands: (left) 16 January, (right) 18 February. Dashed line is ''far'' environment that corresponds to hodographs in Figs. 6 and 5, solid line is closer to convective band. The greater modification for 18 February could be related to its greater intensity (cf. Figs. 6 and 5) or lack of movement. Flow is positive toward the rear of the band. Heading-dependent wind biases are negligible, since (a) the 16 January aircraft sounding in Fig. 13 was at constant heading; and (b) the 18 February profile is drawn through the line-normal wind values just outside the convection from reverse-heading legs at four different heights.

generate new convection. This is made possible by the small CIN. From Table 4, CIN's for both GATE (2–3 J kg^{-1}; also see Fig. 13 of ZML for day 257) and COARE (typically $<$10 J kg^{-1}) are minute compared to midlatitudes values of $\sim$60–100 J kg^{-1} reported by Bluestein et al. (1987) for nonsevere Oklahoma convective bands. Also, the photographs of line leading edges in LeMone et al. (1984a) suggest the nearly continuous generation of new convection one would expect with little or no CIN.

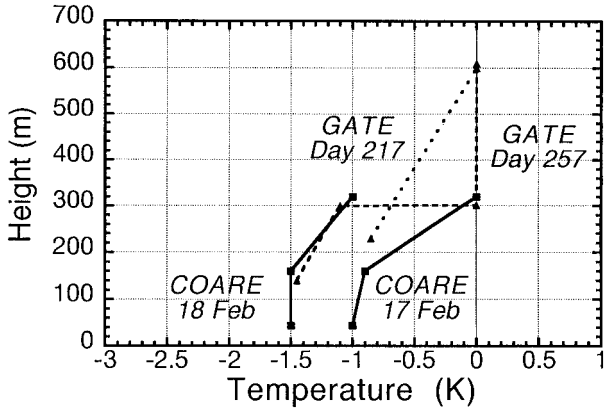

FIG. 14. Temperature deficit ΔT (relative to environment) for the cold pools associated with convective bands on COARE days 17 February and 18 February, and GATE days 257 and 217, based on aircraft penetrations.

It is likely that small convective inhibition enables the convective bands of days 217 and 257 to persist for hours without optimal forcing as described in RKW. Indeed, these bands are suboptimal if vertical velocity is a measure: even for similar CAPEs, the GATE systems have surprisingly weak vertical velocities compared to midlatitude and tropical continental storms (Zipser and LeMone 1980; Lucas et al. 1994). Thus it is not surprising that these convective bands do not even satisfy the assumptions RKW use in deriving their criteria for optimal forcing [their Eq. (10)]. That is, (i) the leading-edge updrafts are not vertical (LeMone et al. 1984a), (ii) the convective-band propagation speed does not match the wind speed at any low level (LeMone et al. 1984b), and (iii) the environmental line-normal shear on day 257 is near zero (LeMone et al. 1984b). In the last instance, the band matches better the idealization in RKW's Eq. (8). Finally, the ratio of the depth of the shear on day 217 [2 km, from Fig. 14, LeMone et al. (1984b), and aircraft data at 100–600 m] to the depth of the cold pool ($\leq$600 m) is larger than in the RKW scenario. In both cases, the bands share some features with the less-than-optimal strong cold pool/weak shear case discussed in RKW. However, since tropical

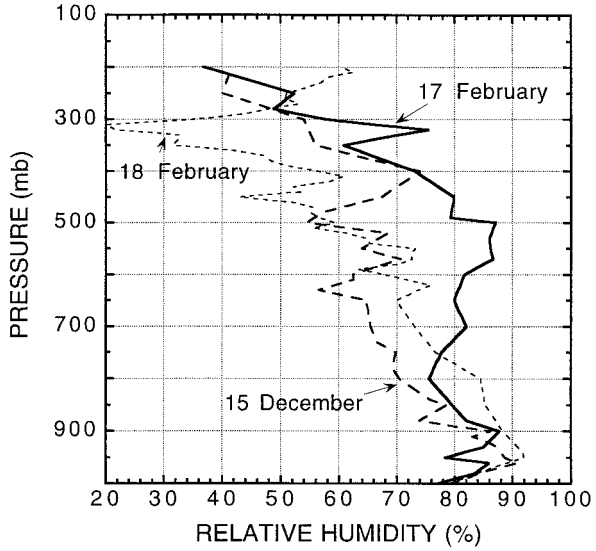

FIG. 15. As in Fig. 12 but for COARE convective bands of 18 February, 15 December, and 17 February. The 18 February bands were short lived [~2 h life cycle according to Hildebrand (1998)] and occurred in sequence; 17 February bands coexisted and lasted at least 3 hours. 15 December bands evolved in a similar manner to the 18 February bands.

oceanic cold pools are weak and shallow compared to midlatitude continental cold pools, there should be differences. For example, as suggested by LeMone et al. (1984a), low pressure created by the wedge of warm air formed by successively older rising plumes (that have risen successively higher) as one moves rearward from the leading edge, may play a relatively more important role in tilting the leading edge updrafts rearward than in the RKW case, where the downdraft dominates.

Longer-lived slower-moving lines appear to be favored by high relative humidities between the top of the boundary layer and 500 mb. Relative humidities in this layer were of the order of 80% for both the GATE slow-movers, including day 257 (Fig. 13; ZML), higher than for the GATE fast-movers or the COARE MCS (Fig. 12). Higher relative humidities at these levels reduce the deleterious effects of entrainment (e.g., Nicholls et al. 1988), which are likely to have a greater impact in tropical marine convection than for midlatitude continental convection, since convective cores are smaller and buoyancy at lower altitudes is less than for midlatitudes (Lucas et al. 1994).

The behavior of the TOGA COARE 17 and 18 February bands is consistent with this scenario. The 17 February bands coexisted for at least 3 h, whereas those of 18 February lasted ~2 h and occurred in succession, with a new east–west band growing to the south as the old one dissipated (Hildebrand 1998). The 17 February environmental sounding (Fig. 15) is similar to that for the GATE slow-movers, with high environmental relative humidities below 500 mb (Fig. 12); and, like days 217 and 257, the 17 February system has a weak cold pool (Fig. 14). The CIN is -7 J kg^{-1} (Table 4). The 18 February system has a weak cold pool and low CIN but environmental relative humidities are lower than for the more persistent lines in GATE or 17 February above about 750 mb (Fig. 15). Similarly, (i) the short-lived slow-moving bands of 15 December occur in a relatively dry environment (Fig. 15), (ii) the short-lived secondary bands of 12 December had environmental relative humidities dropping to 66% at 650 mb and 45% at 550 mb, and (iii) although the shear-parallel bands of 6 November, 16 January, and 17 January were not documented through their life cycles, all appeared to be short-lived (Table 2). The January bands both had relatively dry environments: on 16 January the environmental relative humidity dropped from 88% at 850 mb to 50% at 510 mb and on 17 January there was a dry layer between 800 and 600 mb, with relative humidities between 66% and 76%. The environment on 6 November was slightly moister, but not as moist as 17 February, with relative humidities that remained in the low 70s between 750 to 700 mb and then increased with height 80% at 650 mb.

We conclude that if shear conditions favor formation of slow-moving lines, they will be longer-lived in environments with high relative humidities below about 500 mb. They can propagate with weak cold-pool forcing because of low CIN. Conversely, we suggest that lower relative humidities between the top of the mixed layer and 500 mb shorten the life of slow lines. This leads to the production of strong cold pools as the systems die. These cold pools, too strong to be held back by the environmental wind, surge out and produce new lines as discussed by Thorpe et al. (1982) and RKW. This is one possible explanation for jumping lines. However, Srivastiva et al. (1986) and Trier et al. (1991) have demonstrated that convective systems can propagate in jumps by means other than cold pools. In some cases, gravity waves are a likely mechanism (e.g., Matejka and Stossmeister 1986; Mapes 1993).

5. Conclusions

a. Summary

The proximity soundings in the vicinity of 19 examples of deep precipitating convection in TOGA COARE extend our knowledge of the role of the environment in determining the mesoscale convective structure. While the vertical shear of the horizontal wind has a clear effect on horizontal organization, thermodynamics are related to convection depth and longevity.

For a uniform environment with adequate large-scale forcing, shear has the dominant effect on or-

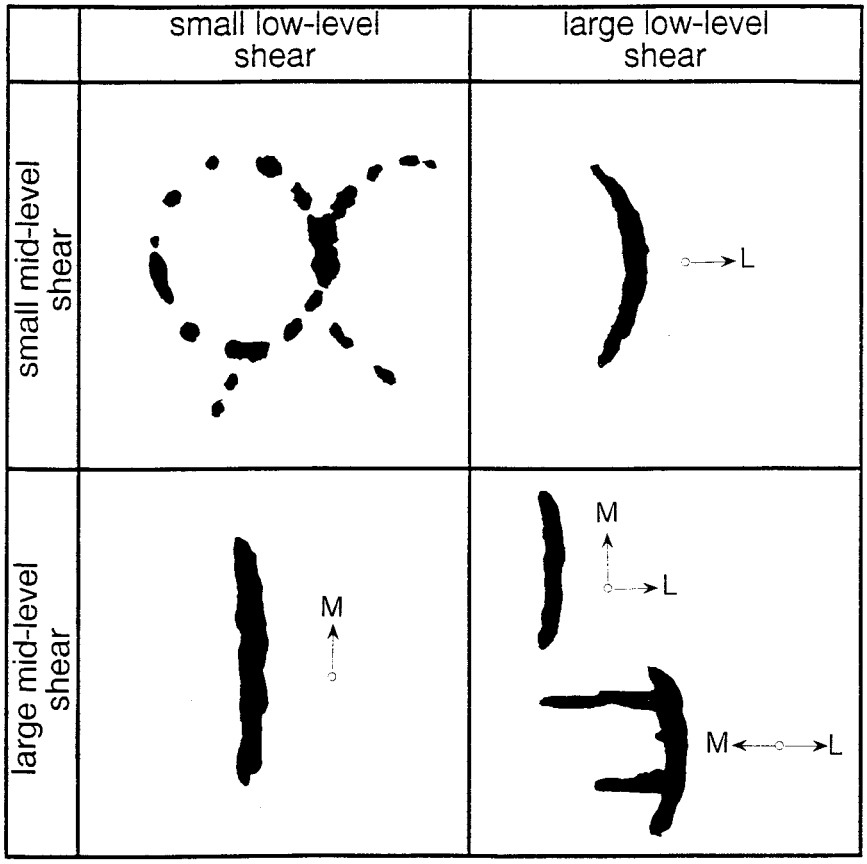

FIG. 16. For convection in a homogeneous environment, schematic showing expected convective structure on the mesoscale, given vertical shear in a lower layer (1000–800 mb) and middle levels (800–400 mb), based on COARE observations and cited works. Length of schematic convective bands is ~100–300 km; line segments in upper-left frame are up to ~50 km in length. Cutoff between ''strong'' and ''weak'' shear for lower layer: 4 m s^{-1} from 1000 to 800 mb (2 m s^{-1} per 100 mb); for upper layer: 5 m s^{-1} from 800 to 400 mb (1.25 m s^{-1} per 100 mb). Arrows marked **L** are shear vectors for the lower layer; arrows marked **M** are shear vectors for the upper layer.

ganization of deep convection on the mesoscale. The relationship of environmental shear to convective structure, based on this and previous studies, is illustrated in Fig. 16. The orientation of the primary convective band is determined by the shear in the lowest 200 mb if the wind difference through that layer exceeds 4 m s^{-1} (2 m s^{-1} for each 100 mb, upper and lower right frames). Secondary lines parallel to the low-level shear can form in front of these systems, although this does not always occur. In the absence of strong low-level shear, lines form parallel to the shear from 800 to 400 mb if the wind difference through that layer exceeds 5 m s^{-1} (1.25 m s^{-1} per 100 mb), as suggested by Alexander and Young (1992) for convection in EMEX (lower-left frame). When the vertical shear exceeds the thresholds in both layers (lower-right frame), the primary band will be normal to the low-level shear, and the direction of the midlevel shear determines whether trailing secondary bands will be present. For midlevel shear in the opposite direction from the low-level shear, secondary bands aligned parallel to the direction of the midlevel shear will extend rearward from the primary band after 3–4 h. MCS structure can become quite complex. For midlevel shear normal to the low-level shear (along the axis of the primary band), the primary band will remain two-dimensional. In the absence of strong shear in either level (upper-left frame), convection will be ''random'' or consist of short-lived line segments whose orientation is determined by cold pools of previously existing systems or some other external forcing.

The shear-perpendicular versus shear-parallel classification is a fuzzy one. It could be sharper for lines earlier in their life cycles, or if shear criteria were better matched to features in the hodograph. Here, for example, the wind shear between 1000 mb and the low-level wind maximum was a better predictor of shear-normal alignment than the 1000–800-mb criterion. However, whether or not the shear-perpendicular bands are exactly perpendicular to the low-level shear, they occur in environments with jetlike profiles,

travel with the speed of the jet maximum, and have substantial mass flux coming in from the front.

Figure 16 does not apply to widespread convection because widespread cold pools in various stages of recovery complicate forcing of new convection. Such behavior has been discussed in the literature in the midlatitude context: Blanchard (1990) and Houze et al. (1990) both associate less-organized convection with cold air near the ground, most often beneath a frontal surface. Gravity waves could complicate structure as well.

Although the vertical distribution of temperature and humidity does not seem to affect the mesoscale convective pattern, it affects COARE convection in other ways. The convection in the COARE region is the deepest on earth (Webster and Lukas 1992), consistent with high parcel equilibrium levels (Table 4), which reach near 100 mb in some cases. The greater depth between the level of free convection and the equilibrium level results in larger CAPEs compared to GATE; however, buoyancies integrated between the top of the mixed layer and 500 mb (500-mb CAPEs) are similar. CINs, with values $\leq$10 J kg^{-1}, are only slightly larger than for GATE (2–3 J kg^{-1}), but much smaller than those reported for midlatitude convection (60–100 J kg^{-1}; Bluestein et al. 1987). These small convective inhibitions enable convection to develop with only weak forcing. The environmental relative humidities are lower than those for GATE slow lines between the top of the mixed layer and 500 mb; this appears to shorten the lifetimes of the COARE shear-parallel convective bands compared to GATE slow-moving bands.

Most of the convective systems studied occur in the rising-air phase of the ISO preceding the maximum low-level westerlies, with west winds at low levels and easterlies at the highest levels. Typically, there is positive zonal shear in the lowest 100–300 mb. Only three systems are in the rising-air phase of the ISO with easterly winds and easterly shear at the lowest levels. There is significant meridional shear at low to middle levels in about half. Consistent with this, COARE convective bands sampled by the aircraft move in all directions, and only 20% have a motion component toward the west. This suggests that the westward cloud-cluster motion seen in satellite infrared images (e.g., Nakazawa 1988) is not due to convective-band propagation. Rather, either new convection forms to the west of old convection or, as implied by the strong easterlies in the wind hodographs, the images reveal westward advection of anvil cloud.

b. Implications

Parameterization of momentum transport by convection. From the foregoing, there is a relationship of convective-band occurrence and alignment to the vertical shear of the horizontal wind, so quasi-two-dimensional systems can be predicted for uniform environments. The systems with wind profiles that have a low-level jet tend to be normal to the shear beneath the jet and move with the speed of the jet. For the shear-perpendicular cases, hodographs imply front-to-rear flow into the line at all levels, leading to, according to Moncrieff (1992), the greatest front-to-rear acceleration as the front-to-rear current is squeezed vertically above the rear downdraft. This results in the largest possible total vertical transport of horizontal momentum for given environmental conditions if processes are two-dimensional and match this theory. However, we have defined ''normal'' as $\pm$30°, too large a range to be useful, with the larger departures from normal believed to be associated with system age. Further, unless the midlevel shear vector is nearly parallel to the line axis, shear-normal convective bands can become increasingly three-dimensional with age, which leads to significant system-scale departures from the two-dimensional momentum-transport idealization (Trier et al. 1998). Also, systems parallel to the midlevel wind do not move in a way simply related to the wind profile, and are often short-lived. Some of the short-lived lines, as suggested by Hildebrand (1998), have radically different momentum-transport properties from those that propagate continuously. Finally, mesoscale organization ceases becoming predictable from a point or area-average sounding once convection is widespread.

Generality. The relative fractions of various types of mesoscale organization strictly apply only to the sample herein. However, earlier studies based on observations (Barnes and Sieckman 1984; Alexander and Young 1992; Keenan and Carbone 1992), modeling/theory (RKW; Thorpe et al. 1982), and theory (Moncrieff 1978, 1981) indicate that the organizing power of environmetal shear has more general application. For example, the larger fraction of random-looking convection in COARE compared to GATE is consistent with a higher frequency of days with weak vertical shear. Similarly, the greater fraction of banded convection in COARE that is shear perpendicular is probably related to a greater frequency of wind profiles with strong shear below a low-level jet. Even so, environmental wind profiles assume secondary importance in the presence of strong external forcing, a common occurrence in the midlatitudes and not unknown in the Tropics.

Acknowledgments. This paper benefited from interactions with several people, which included supplying the authors with impressions of GATE and COARE, and references to the relevant literature. Nearly daily conversations with David Jorgensen, Tom Matejka, and Bradley Smull helped germinate and nurture arguments in this paper; also Peter Hildebrand, Robert Houze Jr., Joanne Simpson, Wei-Kuo Tao, Gary Barnes, Xiaoqing Wu, and Garpee Barleszi

provided encouragement and useful information. John Dougherty provided the radar composites we used for tracking systems away from the ship radars and for Figs. 1–9. William Skamarock, Thomas Matejka, Gary Barnes, David Parsons, and two anonymous reviewers made useful comments on the paper, contributing to its clarity. This work was made possible by the dedication and hard work of the flight and science crews of the NOAA P3s, the NCAR Electra, and the NASA DC-8, and the support people in Townsville and Honiara during TOGA COARE, as well as the radiosonde crews on ships and islands. LeMone and Trier acknowledge the support of NCAR and NSF Grant ATM921550; Zipser, NASA Grant NAG5-1569 and partial support from NCAR during the summer months.

REFERENCES

Alexander, G. D., and G. S. Young, 1992: The relationship between EMEX mesoscale precipitation feature properties and their environmental characteristics. *Mon. Wea. Rev.,* **120,** 554–564.

Arkell, R., and R. Hudlow, 1977: *GATE International Meteorological Radar Atlas.* Center for Experiment Design and Data Analysis, NOAA, 222 pp. [Available from Superindent of Documents, U.S. Govt. Printing Office, Washington, DC 20402.]

Asai, T., 1970: Stability of a plane parallel flow with variable vertical shear and unstable stratification. *J. Meteor. Soc. Japan,* **48,** 129–139.

Balaji, V., J.-L. Redelsperger, and G. P. Klaasen, 1993: Mechanisms for the mesoscale organization of tropical cloud clusters in GATE Phase III. Part I: Shallow cloud bands. *J. Atmos. Sci.,* **50,** 3571–3589.

Barnes, G. M., and K. Sieckman, 1984: The environment of fast- and slow-moving tropical mesoscale convective cloud lines. *Mon. Wea. Rev.,* **112,** 1782–1794.

Betts, A. K., R. W. Grover, and M. W. Moncrieff, 1976: Structure and motion of tropical squall-lines over Venezuela. *Quart. J. Roy. Meteor. Soc.,* **102,** 395–404.

Blanchard, D. O., 1990: Mesoscale convective patterns of the southern high plains. *Bull. Amer. Meteor. Soc.,* **71,** 994–1005.

Bluestein, H. B., and M. H. Jain, 1985: Formation of mesoscale lines of precipitation: Severe squall lines in Oklahoma during the spring. *J. Atmos. Sci.,* **42,** 1711–1732.

——, G. T. Marx, and M. H. Jain, 1987: Formation of mesoscale lines of precipitation: Non-severe squall lines in Oklahoma during the spring. *Mon. Wea. Rev.,* **115,** 2719–2727.

Bolton, D., 1980: The computation of equivalent potential temperature. *Mon. Wea. Rev.,* **108,** 1046–1053.

Carbone, R. E., 1982: A severe frontal rainband. Part I: Stormwide hydrodynamic structure. *J. Atmos. Sci.,* **39,** 258–279.

Chisholm, A. J., and J. H. Renick, 1972: The kinematics of multicell and supercell Alberta hailstorms. Hail Studies Report No. 72-2, Alberta Hail Studies, Research Council of Alberta, 53 pp.

Clark, T. L., T. Hauf, and J. P. Kuettner, 1986: Convective-forced internal gravity waves: Results from two-dimensional experiments. *Quart. J. Roy. Meteor. Soc.,* **112,** 899–926.

Cole, H. L., and E. Miller, 1995: A correction for low-level radiosonde temperature. Preprints, *Ninth Symp. on Meteorological Observations and Instrumentation,* Charlotte, NC, Amer. Meteor. Soc., 32–39.

Dickey, J. A., 1996: Analysis of the atmospheric mixed layer over the western Pacific warm pool. Dept. of Atmos. Sci. Paper No. 609, Colorado State University, 84 pp. [Available from Dept. of Atmospheric Science, Colorado State University, Fort Collins, CO 80523.]

Dudhia, J., and M. W. Moncrieff, 1987: A numerical simulation of quasi-stationary tropical convective bands. *Quart. J. Roy. Meteor. Soc.,* **113,** 929–967.

Etling, D., and R. A. Brown, 1993: Roll vortices in the planetary boundary layer: A review. *Bound.-Layer Meteor.,* **65,** 215–248.

Fairall, C. W., E. F. Bradley, D. P. Rogers, J. B. Edson, and G. S. Young, 1996: Bulk parameterization of air–sea fluxes for the Tropical Ocean Global Atmosphere Coupled Ocean–Atmosphere Response Experiment. *J. Geophys. Res.,* **101,** 3747–3765.

Fitzjarrald, D. R., and M. Garstang, 1981: Vertical structure of the tropical boundary layer. *Mon. Wea. Rev.,* **109,** 1512–1526.

Gamache, J. F., and R. A. Houze Jr., 1982: Mesoscale air motions associated with a tropical squall line. *Mon. Wea. Rev.,* **110,** 118–135.

——, and ——, 1983: Water budget of a mesoscale convective system in the tropics. *J. Atmos. Sci.,* **40,** 1835–1850.

——, and ——, 1985: Further analysis of the composite wind and thermodynamic structure of the 12 September GATE squall line. *Mon. Wea. Rev.,* **113,** 1241–1259.

Geldmeier, M. F., and G. M. Barnes, 1997: The ''footprint'' under a decaying tropical mesoscale convective system. *Mon. Wea. Rev.,* **125,** 2879–2895.

Halverson, J. B., B. S. Ferrier, J. Simpson, and W.-K. Tao, 1996: Two-dimensional numerical modeling investigation of the February 11, 1993 TOGA COARE mesoscale convective system. Preprints, *Seventh Conf. on Mesoscale Processes,* Reading, United Kingdom, Amer. Meteor. Soc., 165–167.

Hildebrand, P., 1998: Shear-parallel moist convection over the tropical ocean: A case study from 18 February 1993 TOGA COARE. *Mon. Wea. Rev.,* **126,** 192–216.

——, W.-C. Lee, C. A. Walther, C. Frush, M. Randall, E. Loew, R. Neitzel, R. Parsons, J. Testud, F. Baudin, and A. LeCornec, 1996: The ELDORA/ASTRAIA Airborne Doppler Weather Radar: High-resolution observations from TOGA-COARE. *Bull. Amer. Meteor. Soc.,* **77,** 213–232.

Hobbs, P. A., and P. O. G. Perrson, 1982: The mesoscale and microscale structure and organization of clouds and precipitation in midlatitude cyclones. Part V: The substructure of narrow cold-frontal rainbands. *J. Atmos. Sci.,* **39,** 280–295.

Houze, R. A., Jr., 1977: Structure and dynamics of a tropical squall-line system. *Mon. Wea. Rev.,* **105,** 1540–1567.

——, and C.-P. Cheng, 1977: Radar characteristics of tropical convection observed during GATE. *Mon. Wea. Rev.,* **105,** 964–980.

——, and E. N. Rappaport, 1984: Air motions and precipitation of an early summer squall line over the eastern tropical Atlantic. *J. Atmos. Sci.,* **41,** 553–574.

——, B. F. Smull, and P. Dodge, 1990: Mesoscale organization of springtime rainstorms in Oklahoma. *Mon. Wea. Rev.,* **118,** 613–654.

Hu, J., and G. M. Barnes, 1994: A fast-moving MCS parallel to the environmental shear over the oceanic warm pool. Preprints, *Sixth Conf. on Mesoscale Processes,* Portland, OR, Amer. Meteor. Soc., 33–35.

Johnson, R. H., and M. E. Nicholls, 1983: A composite analysis of the boundary layer accompanying a tropical squall line. *Mon. Wea. Rev.,* **111,** 308–319.

Jorgensen, D. P., M. A. LeMone, and S. B. Trier, 1997: Structure and evolution of the 22 February 1993 TOGA COARE squall line: Aircraft observations of precipitation, circulation, and surface energy fluxes. *J. Atmos. Sci.,* **54,** 1961–1985.

Keenan, T. D., and R. E. Carbone, 1992: A preliminary morphology of precipitation systems in tropical northern Australia. *Quart. J. Roy. Meteor. Soc.,* **118,** 283–326.

Kingsmill, D. E., and R. A. Houze Jr., 1998a: Inflow and outflow

characteristics of convection in TOGA COARE. Part I: Velocity structures. *Quart. J. Roy. Meteor. Soc.,* in press.
——, and ——, 1998b: Inflow and outflow characteristics of convection in TOGA COARE. Part II: Thermodynamics. *Quart. J. Roy. Meteor. Soc.*, in press.
Koch, S. E., 1984: The role of an apparent mesoscale frontogenetic circulation in squall line initiation. *Mon. Wea. Rev.,* **112,** 2090–2111.
Krishnamurti, T. N., V. Wong, H. L. Pan, G. Van Dam, and D. McClellan, 1976: Sea surface temperatures for GATE. Report No. 76-3, Dept. of Meteorology, The Florida State University, 268 pp. [Available from Dept. of Meteorology, The Florida State University, Tallahassee, FL 32306.]
Lau, K.-M., L. Peng, C.-H. Sui, and T. Nakazawa, 1989: Dynamics of super cloud clusters, westerly wind burst, 30–60 day oscillation, and ENSO: An unified view. *J. Meteor. Soc. Japan,* **67,** 205–219.
Leary, C. A., 1984: Precipitation structure of the cloud clusters in a tropical easterly wave. *Mon. Wea. Rev.,* **112,** 313–325.
——, and R. A. Houze Jr., 1979a: The structure and evolution of convection in a tropical cloud cluster. *J. Atmos. Sci.,* **36,** 437–457.
——, and ——, 1979b: Melting and evaporation of hydrometeors in precipitation from the anvil clouds of deep tropical convection. *J. Atmos. Sci.,* **36,** 669–679.
LeMone, M. A., 1983: Momentum transport by a line of cumulonimbus. *J. Atmos. Sci.,* **40,** 1815–1834.
——, and R. J. Meitin, 1981: Mesoscale motion fields associated with a slowly moving GATE convective band. *J. Atmos. Sci.,* **38,** 1725–1750.
——, and M. W. Moncrieff, 1994: Momentum and mass transport by convective bands: Comparisons of highly idealized dynamical models to observations. *J. Atmos. Sci.,* **51,** 281–305.
——, G. M. Barnes, E. J. Szoke, and E. J. Zipser, 1984a: The tilt of the leading edge of mesoscale tropical convective lines. *Mon. Wea. Rev.,* **112,** 512–519.
——, ——, and E. J. Zipser 1984b: Momentum fluxes by lines of cumulonimbus over the tropical oceans. *J. Atmos. Sci.,* **41,** 1914–1932.
Lewis, S. A., M. A. LeMone, and D. P. Jorgensen, 1998: Evolution and dynamics of a late-stage squall line that occurred on 20 February 1993, during TOGA COARE. *Mon. Wea. Rev.,* **126,** 3189–3212.
Lin, X., and R. H. Johnson, 1996: Kinematic and thermodynamic characteristics of the flow over the western Pacific warm pool during TOGA COARE. *J. Atmos. Sci.,* **53,** 695–715.
Lucas, C., and E. J. Zipser, 1996: The variability of vertical profiles of wind, temperautre, and moisture during TOGA COARE. Preprints, *Seventh Conf. on Mesoscale Processes,* Reading, United Kingdom, Amer. Meteor. Soc., 125–127.
——, ——, and M. A. LeMone, 1994: Vertical velocity in oceanic convection off tropical Australia. *J. Atmos. Sci.,* **51,** 3183–3103.
Madden, R. A., and P. Julian, 1972: Description of global scale circulation cells in the tropics with a 40–50 day period. *J. Atmos. Sci.,* **29,** 1109–1123.
Malkus, J. S., 1958: On the structure of the trade wind moist layer. Papers Phys. Ocean Meteor. 13, Woods Hole Oceanographic Institution, 47 pp. [Available from Woods Hole Oceanographic Institution, Woods Hole, MA 02543.]
——, and H. Riehl, 1964: Cloud structure and distributions over the tropical Pacific Ocean. *Tellus,* **16,** 275–287.
Mapes, B. E., 1993: Gregarious tropical convection. *J. Atmos. Sci.,* **50,** 2026–2037.
——, and R. A. Houze Jr., 1993: Cloud clusters and superclusters over the oceanic warm pool. *Mon. Wea. Rev.,* **121,** 1398–1415.
——, and P. Zuidema, 1996: Radiative–dynamical consequenes of dry tongues in the tropical troposphere. *J. Atmos. Sci.,* **53,** 620–638.
Martin, D. W., and A. J. Schreiner, 1981: Characteristics of west African and east Atlantic cloud clusters: A survey from GATE. *Mon. Wea. Rev.,* **109,** 1671–1688.
Matejka, T., and G. Stossmeister, 1986: Convective–mesoscale interaction in a squall line. Preprints, *23d Conf. on Radar Meteorology and Conf. on Cloud Physics,* Vol. III, Snowmass, CO, Amer. Meteor. Soc., J135–J138.
——, and S. A. Lewis, 1997: Improving research aircraft navigation by incorporating INS and GPS information in a variational solution. *J. Atmos. Oceanic Technol.,* **14,** 495–511.
Moncrieff, M. W., 1978: The dynamical structure of two-dimensional steady convection in constant vertical shear. *Quart. J. Roy. Meteor. Soc.,* **104,** 543–567.
——, 1981: A theory of organised steady convection and its transport properties. *Quart. J. Roy. Meteor. Soc.,* **107,** 29–50.
——, 1992: Organised mesoscale convective systems: Archetypal dynamical models, mass and momentum flux theory, and parametrisation. *Quart. J. Roy. Meteor. Soc.,* **118,** 819–850.
——, and J. S. A. Green, 1972: The propagation and transfer properties of steady convective overturning in shear. *Quart. J. Roy. Meteor. Soc.,* **98,** 336–352.
——, and M. J. Miller, 1976: The dynamics and simulation of tropical cumulonimbus and squall lines. *Quart. J. Roy. Meteor. Soc.,* **102,** 373–394.
Nakazawa, T., 1988: Tropical superclusters within intraseasonal variations over the western Pacific. *J. Meteor. Soc. Japan,* **66,** 823–839.
Newton, C. W., 1950: Structure and mechanism of the prefrontal squall line. *J. Meteor.,* **7,** 210–222.
——, 1963: Dynamics of severe convective storms. *Severe Local Storms, Meteor. Monogr.,* No. 27, Amer. Meteor. Soc., 33–58.
Nicholls, M. E., R. H. Johnson, and W. R. Cotton, 1988: The sensitivity of two-dimensional simulations of tropical squall lines to environmental profiles. *J. Atmos. Sci.,* **45,** 3626–3649.
Nicholls, S., and M. A. LeMone, 1980: The fair weather boundary layer in GATE: The relationship of subcloud fluxes and structure to the distribution and enhancement of cumulus clouds. *J. Atmos. Sci.,* **37,** 2051–2067.
——, ——, and G. Sommeria, 1982: The simulation of a fair weather marine boundary layer in GATE using a three dimensional model. *Quart. J. Roy. Meteor. Soc.,* **108,** 167–190.
Pandya, R. E., and D. R. Durran, 1996: The influence of convectively generated thermal forcing on the mesoscale circulation around squall lines. *J.Atmos. Sci.,* **53,** 2924–2951.
Pestaina-Haynes, M., and G. L. Austin, 1976: Comparison between maritime tropical (GATE and Barbados) and continental mid-latitude (Montreal) precipitation lines. *J. Appl. Meteor.,* **15,** 1077–1082.
Reed, R. J., D. C. Norquist, and E. E. Recker, 1977: The structure and properties of African wave disturbances as observed during Phase III of GATE. *Mon. Wea. Rev.,* **105,** 317–333.
Rickenbach, T. M., and S. A. Rutledge, 1998: Convection in TOGA COARE: Horizontal scale, morphology, and rainfall production. *J. Atmos. Sci.,* **55,** 2715–2729.
Robe, F. R., 1996a: Sea, sun, and shear: A recipe for precipitating convection, tropical rainbands, and hurricane spiral arms. Ph.D. dissertation, Massachusetts Institute of Technology, 242 pp. [Available from MIT Libraries, Rm. 14-0551, Cambridge, MA 02139-4307.]
——, 1996b: Sea, sun, and shear: A recipe for tropical rainbands. Preprints, *Seventh Conf. on Mesoscale Processes,* Amer. Meteor. Soc., 174–175.
Rotunno, R., J. B. Klemp, and M. L. Weisman, 1988: A theory for strong, long-lived squall lines. *J. Atmos. Sci.,* **45,** 463–485.
Skamarock, W. C., S. B. Trier, and M. A. LeMone, 1996: The dynamics of slow and fast-moving convective lines in TOGA COARE. Preprints, *Seventh Conf. on Mesoscale Processes,* Reading, United Kingdom, Amer. Meteor. Soc., 301–303.

Smull, B. F., T. J. Matejka, and M. A. LeMone, 1996: Airflow trajectories within a slow-moving convective system observed during TOGA-COARE. Preprints, *Seventh Conf. on Mesoscale Processes,* Reading, United Kingdom, Amer. Meteor. Soc., 289–291.

Srivastiva, R. C., T. J. Matejka, and T. J. Lorello, 1986: Doppler radar study of the trailing anvil region associated with a squall line. *J. Atmos. Sci.,* **43,** 356–377.

Sun, W.-Y., 1978: Stability analysis of deep cloud streets. *J. Atmos. Sci.,* **35,** 466–483.

Thorpe, A. J., M. J. Miller, and M. W. Moncrieff, 1982: Two-dimensional convection in non-constant shear: A model of mid-latitude squall lines. *Quart. J. Roy. Meteor. Soc.,* **108,** 739–762.

Trier, S. B., D. B. Parsons, and J. H. E. Clark, 1991: Environment and evolution of a cold-frontal mesoscale convective system. *Mon. Wea. Rev.,* **119,** 2429–2455.

——, W. C. Skamarock, M. A. LeMone, D. B. Parsons, and D. P. Jorgensen, 1996: Structure and evolution of the 22 February 1993 TOGA-COARE squall line: Numerical simulations. *J. Atmos. Sci.,* **53,** 2861–2886.

——, ——, and M. A. LeMone, 1997: Structure and evolution of the 22 Feburary 1993 TOGA COARE squall line: Organization mechanisms inferred from numerical simulation. *J. Atmos. Sci.,* **54,** 386–407.

——, M. A. LeMone, and W. C. Skamarock, 1998: Effect of three-dimensional structure on the stormwide horizontal accelerations and momentum budget or a simulated squall line. *Mon. Wea. Rev.,* **126,** 2580–2598.

Webster, P. J., and R. Lukas, 1992: TOGA COARE: The Coupled Ocean–Atmosphere Response Experiment. *Bull. Amer. Meteor. Soc.,* **73,** 1377–1416.

Wei, T., and R. A. Houze Jr., 1987: The GATE squall line of 9–10 August 1974. *Adv. Atmos. Sci.,* **4,** 85–92.

Weisman, M. L., and J. B. Klemp, 1982: The dependence of numerically simulated convective storms on vertical wind shear and buoyancy. *Mon. Wea. Rev.,* **110,** 504–520.

——, and ——, 1984: The structure and classification of numerically simulated convective storms in directionally varying wind shears. *Mon. Wea. Rev.,* **112,** 2479–2498.

——, and ——, 1986: Characteristics of convective storms. *Mesoscale Meteorology and Forecasting,* P. S. Ray, Ed., Amer. Meteor. Soc., 331–358.

Yuter, S. E., R. A. Houze Jr., B. F. Smull, F. D. Marks Jr., J. R. Daugherty, and S. R. Brodzik, 1995: TOGA COARE aircraft mission summary images: An electronic atlas. *Bull. Amer. Meteor. Soc.,* **76,** 319–328.

Zipser, E. J., and M. A. LeMone, 1980: Cumulonimbus and vertical events in GATE. Part II: Synthesis and model core structure. *J. Atmos. Sci.,* **37,** 2458–2469.

——, and R. H. Johnson, 1998: Systematic errors in radiosonde humidities. A global problem? Preprints, *10th Symp. on Meteorological Observations and Instrumentation,* Phoenix, AZ, Amer. Meteor. Soc., 72–73.

——, R. J. Meitin, and M. A. LeMone, 1981: Mesoscale motion fields associated with a slowly moving GATE convective band. *J. Atmos. Sci.,* **38,** 1725–1750.

——, Y.-L. Chen, and E. J. Szoke, 1983: On the generation of heavy precipitation with the anvil system of a tropical squall line. *Proc. 21st Conf. on Radar Meteorology,* Edmonton, AB, Canada, Amer. Meteor. Soc., 50–56.